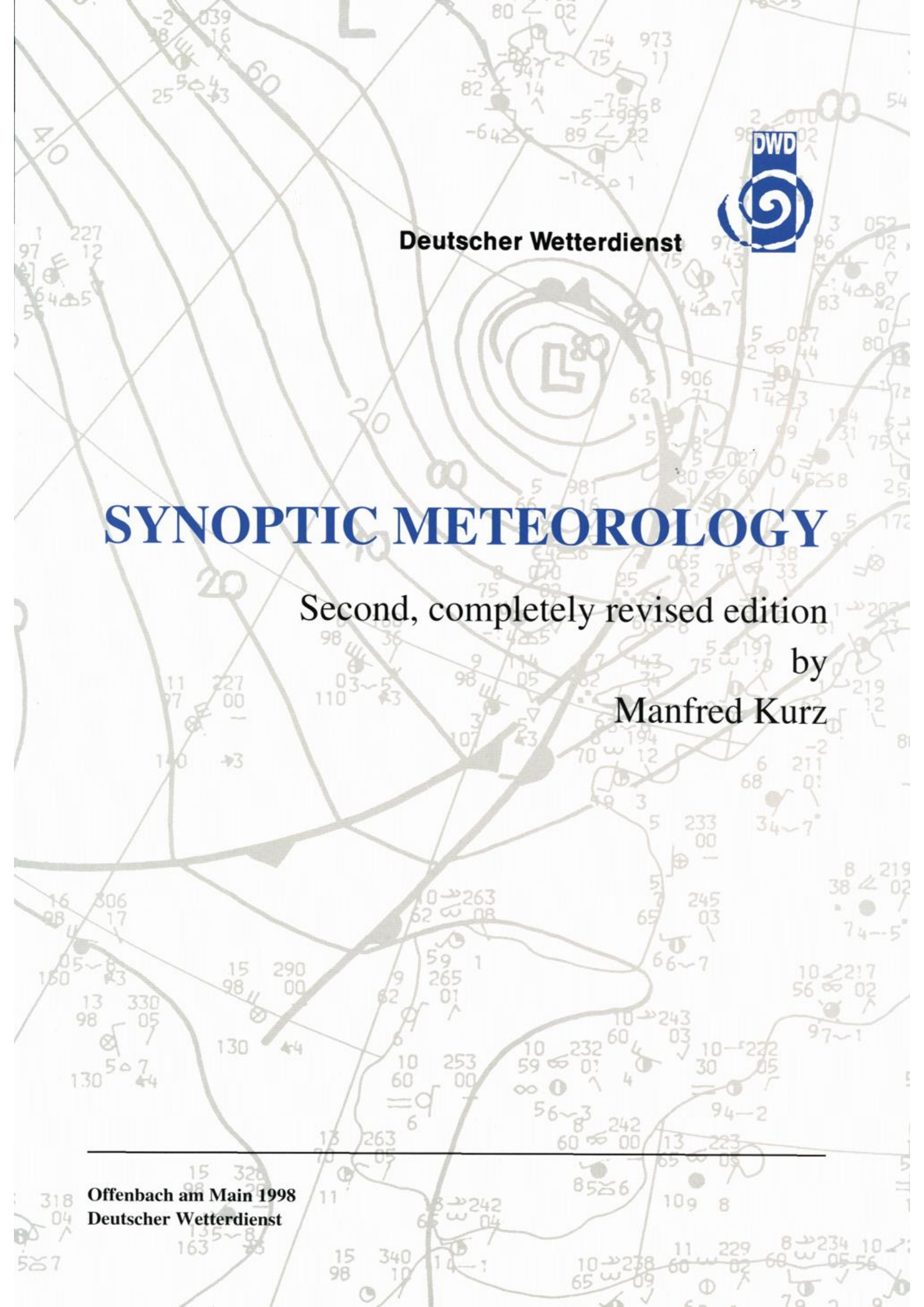

Deutscher Wetterdienst

SYNOPTIC METEOROLOGY

Second, completely revised edition

by

Manfred Kurz

Offenbach am Main 1998
Deutscher Wetterdienst

Training Guidelines of the
GERMAN METEOROLOGICAL SERVICE

8

SYNOPTIC METEOROLOGY

Second, completely revised edition

by

Manfred Kurz

Offenbach am Main 1998
Deutscher Wetterdienst

ISSN 0459-0236
ISBN 3-88148-338-1

Translation from: Manfred Kurz, Synoptische Meteorologie, Leitfäden für die Ausbildung im Deutschen Wetterdienst Nr. 8, Offenbach am Main 1990.

Printed on acid-free paper.

Editor and Publisher:
Deutscher Wetterdienst, Frankfurter Str. 135,
63067 Offenbach am Main, Germany

Address of the author:
Dipl.-Met. Manfred Kurz
Deutscher Wetterdienst
Frankfurter Str. 135
D-63067 Offenbach am Main
Germany

Index

Introduction

"Synoptic meteorology" describes that part of meteorology which is concerned, on the basis of synoptic observations, with the study of meteorological phenomena in regard to their spatial distribution and changes in respect of time and is intended for forecasting the weather (see WMO [1]). For this purpose the relevant meteorological parameters must be observed simultaneously for the same dates, distributed as quickly as possible via a global telecommunications network and then finally processed in a suitable format. This extensive material forms the basis of three-dimensional weather analysis and diagnosis and, as a further extension, weather prediction.

To perform this task a larger organisational apparatus is needed. Therefore operational synoptics is one of the most important tasks of the national meteorological services. Furthermore world wide cooperation of the various services is essential and is therefore organised within the WMO.

Following the introduction of computer processing, a major change in the methods of synoptic meteorology has taken place since about 1960. Today most of the analyses required are produced numerically. But of special importance was the introduction of numerical models in which – based on the relevant equations – the behaviour of the atmosphere is simulated and the state of the meteorological parameters is computed over a certain number of days. The results of these model computations have meanwhile become so accurate that they now form the basis of short-range and medium-range weather forecasting.

The main job of the meteorologist working today in synoptics is therefore to monitor the numerical analyses and, if necessary, correct them, to diagnose physically the momentary state of the atmosphere and to interpret the numerically computed forecasting results in such a way that they can be used. Naturally it is necessary time after time to derive weather forecasts in the case of obvious false prognosis from the models independently from the numerical methods. In order to be able to undertake this work properly, comprehensive knowledge about the structure and dynamics of the synoptic systems as well as basic theoretical knowledge is necessary. Only if the effective processes in the weather system are known is it possible to extrapolate these in order to achieve permanent success in the future. The object of this guide is to provide the newcomer to the subject of synoptic meteorology with the basic knowledge needed for this.

With regard to the composition of the guide, it should be noted that the first three chapters include the theoretical principles which are necessary to understand the synoptic processes. In chapters 4–9 the most important synoptic structures and systems are described, whilst chapters 10–14 are devoted to the development processes. Chapter 15 contains details about the dynamics of convective weather systems. Finally in chapter 16 some weather situations are given as examples of synoptic developments.

List of symbols

A	horizontal cross section, area
A_E	equatorial projection of an area
$A_{s,\,r,\,t}$	amplitude of streamlines, relative streamlines and trajectories
A_J	amplitude of the jet axis
A_T	temperature advection
$A\eta$	vorticity advection
APE	available potential energy
a	earth's radius
B	half-width
b	three-hour pressure change; crest height of a mountain
C	circulation
c, **c**	speed or speed vector of a moving system
c	phase velocity of waves
c_i, c_r	imaginary and real part of phase velocity
c_F	front velocity
$c_R = \beta\left(\frac{L}{2\pi}\right)^2$	ROSSBY velocity
c_x, c_y	velocity components in x-and y-direction
C_D	drag coefficient
c_p, c_v	specific heat at constant pressure or constant volume
D	thickness, relative topography; horizontal divergence
d	grid spacing
E	deformation
F	area in polar diagram; frontogenesis function; forcing function
F, $\mathbf{F}_3$	horizontal or three-dimensional vector of frictional force
FQ	forcing of vertical motion
$f = 2\,\Omega \sin\varphi$	Coriolis parameter
g	vector of effective gravity
g	gravitational acceleration
H	characteristic height; height of a topography in [m]; heat flux per unit mass and time
h	vertical thickness, layer thickness; height of mountain topography; parameter
I	internal energy
i, j	unit vectors in x or y-direction
K	kinetic energy
$K_{i,s,t}$	curvature of isobars, streamlines and trajectories
K_n	orthogonal curvature
k	wave number; constant
k	vertical unit vector
L	characteristic length; wavelength
L_c	critical wavelength
$L_{s,\,t}$	wavelength of streamline and trajectory
L_s	stationary wavelength; vertical wavelength
l	"half-width" of a mountain
M	mass
m	scale factor; $m = u_g - fy$ absolute momentum
N	number of isobar-isosteric solenoids
n	normal coordinate of the natural coordinate system
n	unit vector in n-direction
P	potential energy; potential vorticity
p	air pressure
Q	heat; air mass characteristic; forcing function
Q	Q vector
q^2	constant
R_d	gas constant for dry air
$R_{i,s,t}$	radius of isobars, streamlines and trajectories
R_n	orthogonal radius
Ri	RICHARDSON number
Ro	ROSSBY number
s	tangential coordinate of the natural coordinate system; scalar magnitude
S	deformation
T	absolute temperature
T_v	virtual temperature
t	time
t	unit vector in s-direction
t_e	e-folding time
TPE	total potential energy
U	horizontal velocity; zonal basic flow
u	wind component in x-direction

u_g, u*	geostrophic, ageostrophic wind component in x-direction
U*	vertical mean of the zonal wind
U_T	thermal wind
V	wind velocity
v, $\mathbf{v}_3$	horizontal and three-dimensional wind vector
v	wind component in y-direction
$\mathbf{v}_g$	vector of geostrophic wind
v*	ageostrophic wind component
v_g, v*	geostrophic, ageostrophic wind component in y-direction
V_G	gradient wind
V_N	normal component of the wind
$\mathbf{v}_T$	thermal wind
W	vertical velocity
w	vertical wind component
w_M	orographically triggered vertical motion
x	horizontal, normally east-pointing coordinate of a Cartesian coordinate system
y	horizontal, normally north-pointing coordinate of a Cartesian coordinate system
$y_{s,r}$	ordinate of the streamline or relative streamline
z	vertical coordinate; geometric height
α	specific volume; angle
β	wind direction; $\beta \equiv \frac{\partial f}{\partial y}$ ROSSBY parameter
γ	angle; function
$\gamma = -\frac{dT}{dz}$	actual vertical temperature gradient
γ_t	dry-adiabatic temperature gradient
γ_f	moist-adiabatic temperature gradient
Δ	difference
δ	differential; variation; discriminant; declination angle
ζ	relative vorticity
ζ_g	geostrophic relative vorticity
ζ_T	thermal vorticity
η	absolute vorticity
η_g	geostrophic absolute vorticity
Θ	potential temperature
Θ_{PS}	pseudo-potential temperature
Λ	function of deformation
ϱ	air density
σ	stability parameter
$\boldsymbol{\tau}$	horizontal vector of drag
Φ	geopotential
φ	geographic latitude
Ψ	MONTGOMERY stream function
ψ	description of gradients for a surface = const.; angle; stream function of ageostrophic circulation
$\boldsymbol{\Omega}$, Ω	angular velocity of earth's rotation (vectorial or scalar)
$\omega = \frac{dp}{dt}$	vertical motion in the p-system
×	vector product
d, ∂	differential
$\nabla = \frac{\partial}{\partial x} + \frac{\partial}{\partial y}$	horizontal Nabla operator
$\nabla_3 = \frac{\partial}{\partial x} + \frac{\partial}{\partial y} + \frac{\partial}{\partial z}$	three-dimensional Nabla operator
$\nabla^2 = \frac{\partial^2}{\partial x^2} + \frac{\partial^2}{\partial y^2}$	Laplace operator

The vectors have been shown in the illustrations by simple letters with an arrow over them and the Nabla operator with a simple ∇.

1 Basic Equations

In this section the most important basic equations which are of importance when examining synoptic systems will be noted briefly and mostly without derivation. Derivations and more exact details can be obtained from the works of HALTINER and MARTIN [2], HOLTON [3], PETTERSSEN [4] and WIN-NIELSEN [5].

1.1 Equations of thermodynamics

The gas equation

$$p\alpha = R_d T$$

or

$$\frac{p}{\varrho} = R_d T \tag{1.1}$$

determines the state of the air as a gas mixture. The equation applies to dry air with pressure p, specific volume α, air density ϱ, temperature T and gas constant R_d. When applying to unsaturated moist air, T must be replaced by virtual temperature T_v.

A spatial configuration in which the surfaces of equal pressure (isobaric surfaces) intersect the surfaces of equal specific volume (isosteric surfaces) is described as baroclinic. According to the gas equation this is also synonymous with the surfaces of equal density and equal temperature intersecting the pressure surfaces.

A configuration in which by contrast all these surfaces are parallel to each other is called barotropic.

If heat dQ is imparted from the environment to an air particle, this is used partially to increase its inner energy and partially for expansion work against the outer pressure (first law of thermodynamics). For the unit mass the following applies

$$dQ = c_v dT + p d\alpha \tag{1.2}$$

or – using (1.1)

$$dQ = c_p dT + \alpha dp. \tag{1.3}$$

c_p, c_v are the specific heats at constant pressure and constant volume.

The most important processes by which diabatic heat transfer occurs in the atmosphere are condensation, radiation and turbulence.

Processes in which the particles neither absorb heat from the environment nor supply heat to it are called adiabatic. Assuming $dQ = 0$, Poisson's equation

$$\frac{T}{T_0} = \left(\frac{p}{p_0}\right)^{R_d/c_p}, \tag{1.4}$$

then results from (1.3) and (1.1) through which the variations of temperature and pressure are coupled with each other during an adiabatic process. If $p_0 = 1000$ hPa is used, (1.4) produces the definition equation of potential temperature

$$\Theta = T\left(\frac{1000}{p}\right)^{R_d/c_p}. \tag{1.5}$$

It is a conservative property for adiabatic processes.

In the case of adiabatic expansion of moist air, water vapour present in the air can condense. At the same time condensation heat is released which reduces adiabatic cooling of the particles. In analogy to potential temperature, several temperatures have been defined, which are conservative for adiabatic processes with inclusion of the condensation. For practical purposes the pseudo-potential temperature Θ_{PS} which can be calculated graphically in a thermodynamic diagram is particularly suitable.

1.2 Equations of motion

The three-dimensional motion of a particle relative to the rotating earth is described with the equation of motion:

$$\frac{d\mathbf{v_3}}{dt} = -\frac{1}{\varrho}\boldsymbol{\nabla}_3 - 2\boldsymbol{\Omega} \times \mathbf{v}_3 + \mathbf{g} + \mathbf{F}_3. \tag{1.6}$$

$\boldsymbol{\nabla}_3$ is the three-dimensional wind vector, $-\boldsymbol{\nabla}_3$ p the three-dimensional pressure gradient, $\boldsymbol{\Omega}$ the vector of the earth's rotation, $\mathbf{g}$ effective gravity and $\mathbf{F}_3$, the vector of frictional force. Corresponding to this equation the individual acceleration of the particle results from the effect of the pressure gradient force, Coriolis force, gravity and frictional force.

By neglecting a relatively small component of Coriolis force which results from the effect of vertical motion, and assuming a frictionless flow, the horizontal equation of motion for the x-, y-plane of a normal Cartesian coordinate system

$$\frac{d\mathbf{v}}{dt} = -\frac{1}{\varrho}\boldsymbol{\nabla}p - f\mathbf{k} \times \mathbf{v} \tag{1.7}$$

with the Coriolis parameter $f = 2\Omega \sin \varphi$ and the vertical unit vector $\mathbf{k}$ results from (1.6). φ is the geographical latitude, $\mathbf{v}$ is the horizontal wind vector, $-\boldsymbol{\nabla}p$ the horizontal pressure gradient.

If the vertical component of the Coriolis force is neglected,

$$\frac{dw}{dt} = -\frac{1}{\varrho}\frac{\partial p}{\partial z} - g \tag{1.8}$$

is obtained for the vertical motion component w along the vertical coordinate z.

For many investigations, it is more helpful to use a so-called natural coordinate system instead of the Cartesian system. Its horizontal coordinates (s, n) are defined by the unit vectors $\mathbf{t}$ and $\mathbf{n}$ whereby $\mathbf{t}$ is arranged parallel to the flow at each point and $\mathbf{n}$ runs perpendicularly to it, positively counted to the left looking along the direction of flow.

In this system the horizontal wind vector is $\mathbf{v} = V\,\mathbf{t}$, whereby $V = \frac{ds}{dt}$ represents the wind velocity.

$$\frac{d\mathbf{v}}{dt} = \frac{dV}{dt}\mathbf{t} + V\frac{d\mathbf{t}}{dt} \tag{1.9}$$

applies for acceleration.

With the aid of Fig 1.1 it is recognised that vector $d\mathbf{t}$ is with its amount equal to the angle change $d\beta$ and runs normal to $\mathbf{t}$. Therefore

$$\frac{d\mathbf{t}}{dt} = \frac{ds}{dt}\frac{d\mathbf{t}}{ds} = V\frac{d\beta}{ds}\mathbf{n} = VK_t\mathbf{n}.$$

is obtained.

Here $K_t = \frac{d\beta}{ds}$ is the curvature of the particle trajectory. Used in (1.9) we obtain

$$\frac{d\mathbf{v}}{dt} = \frac{dV}{dt}\mathbf{t} + V^2 K_t \mathbf{n}$$

or (1.10)

$$\frac{d\mathbf{v}}{dt} = \frac{dV}{dt}\mathbf{t} + \frac{V^2}{R_t}\mathbf{n}$$

if the radius of trajectory $R_t = \frac{1}{K_t}$ is used. K_t and R_t are positive in the case of cyclonic and negative in the case of anticyclonic trajectory curvature.

It is easy to see that the Coriolis term $-f\,\mathbf{k}\times\mathbf{v}$ changes to $-f\,V\mathbf{n}$ in the natural coordinate system. Therefore equation (1.7) can be shown in two component equations for the s and n-axes:

$$\frac{dV}{dt} = -\frac{1}{\varrho}\frac{\partial p}{\partial s}$$

$$\frac{V^2}{R_t} = -\frac{1}{\varrho}\frac{\partial p}{\partial n} - fV \qquad (1.11)$$

dV/dt is the tangential component of acceleration. It describes changes in particle velocity. This requires that pressure differences exist in the direction of motion. With motion towards low pressure the velocity increases, with motion towards high pressure it decreases.

V^2/R_t is the normal or centripetal component of acceleration. It describes changes in the direction of motion of the particle depending on effects of forces working across the trajectory. So that a particle can undergo a change of direction to the left, i.e. pass through a cyclonic trajectory with $R_t > 0$, the pressure gradient force in this direction must outweigh the Coriolis force which always pulls to the right. For a change of direction to the right i.e. passing through an anticyclonic trajectory ($R_t < 0$), the Coriolis force must either work alone (motion of inertia) or it must outweigh the gradient force or both forces must pull in the same direction.

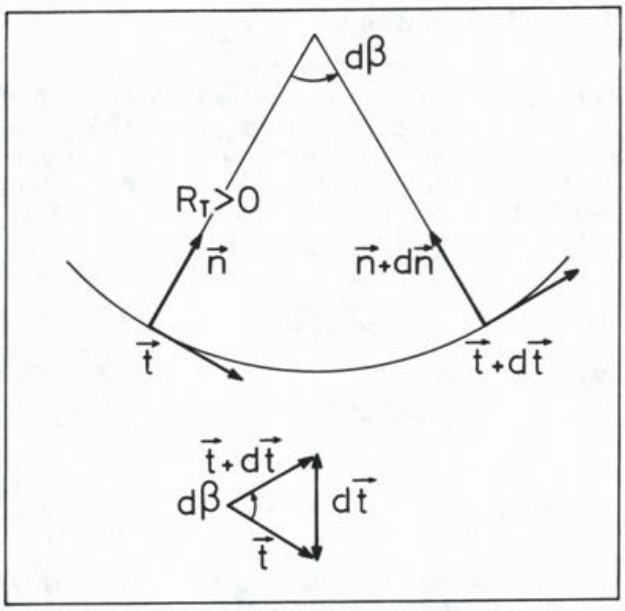

Fig. 1.1
Change from **t** and **n** in the natural coordinate system

2 Relations between wind, pressure and temperature fields

Based on a consideration of the observed dimensions, relations between the various atmospheric fields are derived in this section. In doing so the presentation will be limited to the relations which are relevant for synoptic analysis and diagnosis in middle and high latitudes.

2.1 Order of magnitude of synoptic systems

In the practical use of the equations presented in the first section, difficulties may be met, as many terms are contained in these which either cannot be technically measured or only inaccurately. This applies for example for the acceleration terms in the equations of motion. However, in order to be able to work with the equations, they must be simplified as far as possible by either representing difficult terms approximately or by simply neglecting them. How far this is possible without impairing the statement of the particular equation depends primarily on the dimensions of the phenomena observed.

The classification system of "scales" was created for dimension-related differentiation of the varying types of meteorological phenomena and structures. Here the numerical values for certain characteristic parameters such as length, height, duration, speed etc are compared. The WMO [6] uses the following subdivisions:

a) Small scale (< 100 km); e.g. thunderstorms, local winds, tornadoes

b) Meso scale (100–1000 km); e.g. fronts, convective cloud clusters

c) Large scale (1000–5000 km); e.g. low pressure and high pressure systems

d) Planetary scale (> 5000 km); e.g. long tropospheric waves.

The characteristic length of the dimensional range concerned is quoted in brackets in each case.

In the case of wave-shaped formations, it can be equated approximately with a half wave-length.

Synoptic meteorology is concerned mainly with systems which belong to the "large scale" so that the description "synoptic scale" is also usual for this dimensional range. But also phenomena of the "meso scale" and "planetary scale" belong to the scope of synoptics.

Detailed below are the most important characteristic data for the dimensions of the synoptic scale systems:

Horizontal velocity	U	$\sim 10\,\mathrm{ms}^{-1}$
Vertical velocity	W	$\sim 10^{-2}\,\mathrm{ms}^{-1}$
Length	L	$\sim 10^{6}\,\mathrm{m}$
Height	H	$\sim 10^{4}\,\mathrm{m}$
Ratio of height to length	H/L	$\sim 1/100$
Duration (time scale)	L/U	$\sim 10^{5}\,\mathrm{s} \sim 1$ day

To characterise fluid systems, the ROSSBY number (after the Swedish meterologist C.G. Rossby) is frequently used. It is defined by the ratio of individual acceleration to inertia acceleration i.e. acceleration as a result of the Coriolis force. Using the parameters just listed,

$$\mathrm{Ro} = \frac{\mathrm{U}}{\mathrm{L/U}}\,\frac{1}{\mathrm{fU}} = \frac{\mathrm{U}}{\mathrm{fL}} \tag{2.1}$$

results.

Ro has the dimension 10^{-1} for the "large scale".

2.2 Hydrostatic equilibrium

If the magnitude of various terms in the equations of motion is estimated by means of the data quoted above, the result is that accelerations are one or more to the power of ten less than the effective forces. This applies especially for vertical acceleration dw/dt in (1.8) which with an order of magnitude of $10^{-7}\mathrm{ms}^{-2}$ is minute compared to the terms on the right-hand side which possess the dimension $10\ \mathrm{ms}^{-2}$. This means, however, that in the "large scale" a nearly complete balance between vertical pressure gradient force and gravity can be assumed. This balance is described as hydrostatic equilibrium.

With $\mathrm{dw/dt} = 0$ the hydrostatic equation

$$\mathrm{dp} = -\mathrm{g}\varrho\,\mathrm{dz} \tag{2.2}$$

results from (1.8).

For practical uses of this formula it is helpful to eliminate the variation of g with latitude. This is done by introducing geopotential ϕ as a new variable. It is defined as the energy which is necessary to lift the unit mass from sea level to level z.

$$\Phi = \int_0^{\mathrm{z}} \mathrm{g\,dz} \cong \mathrm{gz} \quad [\mathrm{m^2 s^{-2}}]. \tag{2.3}$$

With this new variable and using the gas equation, (2.2) can be turned into the form

$$\frac{\mathrm{d}\Phi}{\mathrm{dp}} = -\frac{1}{\varrho} = -\frac{\mathrm{R_d T_v}}{\mathrm{p}} \tag{2.4}$$

in which only density or virtual temperature, resp., appear as determining factor.

Besides the unit $[\mathrm{m^2 s^{-2}}]$ the "geopotential meter" unit is used for the geopotential in synoptic practice. It is defined by

$$1\ \mathrm{gpm} = 9{,}8\ \mathrm{m^2 s^{-2}}.$$

For places where g = 9.8 ms^{-2}, numerical agreement between geometric height in [m] and geopotential in [gpm] results.

Assuming hydrostatic equilibrium in the environment, a statement about temperature change is obtained, which receives an adiabatically moved particle in the vertical plane. Where dQ=0 the following is obtained from (1.3)

$$\frac{\mathrm{dT}}{\mathrm{dp}} = \frac{\alpha}{\mathrm{c_p}} = \frac{1}{\varrho\,\mathrm{c_p}}$$

After passing through the height interval dz

$$\mathrm{dp'} = -\mathrm{g}\varrho'\,\mathrm{dz}$$

applies to environmental pressure in accordance with (2.2).

As the pressure field must be continuous, dp'= dp from which

$$-\frac{dT}{dz}=\frac{\varrho'}{\varrho}\frac{\alpha}{c_p}=\frac{T}{T'}\frac{g}{c_p}$$

follows.

If the particle is in thermal equilibrium with the environment, T' = T is also the case and the adiabatic temperature gradient emerges as

$$\gamma_t\equiv\left(-\frac{dT}{dz}\right)_t=\frac{g}{c_p}=0{,}98\,°C/100\,m. \qquad (2.5)$$

The index t describes a dry adiabatic vertical motion. If in the case of rising moist air the condensation level is exceeded, latent heat - as already noted - is released and adiabatic cooling is reduced accordingly. The moist adiabatic temperature gradient γ_f within the rising cloud air mass is therefore always less than the dry adiabatic gradient γ_t.

The difference between dry or moist adiabatic temperature gradients and the actual temperature gradient $\gamma = -dT/dz$ is a measure of the stability of thermal stratification with vertical motions. The following applies for

Unsaturated air		Saturated air
$\gamma > \gamma_t$	Unstable	$\gamma > \gamma_f$
$\gamma = \gamma_t$	Indifferent	$\gamma = \gamma_f$
$\gamma < \gamma_t$	Stable	$\gamma < \gamma_f$

and combined

$\gamma < \gamma_f$	Absolutely stable
$\gamma_t > \gamma > \gamma_f$	Latently unstable
$\gamma > \gamma_t$	Absolutely unstable

In consideration of the potential or pseudo-potential temperature the following similarly is obtained for

Unsaturated air		Saturated air
$\frac{\partial\theta}{\partial z} < 0$	Unstable	$\frac{\partial\theta_{ps}}{\partial z} < 0$
$= 0$	Indifferent	$= 0$
> 0	Stable	> 0

A lapse rate with vertical decrease of pseudo-potential temperature is especially of major importance for convective processes. A similar stratification is also described as potentially unstable. It appears for example if, in the case of only weak thermal stability, very dry air masses lie above moist air. If the total air column is then subject to lifting, the dry air cools dry-adiabatically, the moist air on the contrary after fast saturation cools moist-adiabatically. As a result the entire air column can very quickly become unstable (see 15.1).

2.3 Forms of equilibrium with horizontal motion

If friction is initially neglected which is permitted above the planetary boundary layer, equations (1.7) and (1.11) apply for horizontal motion. If the dimensions of the terms appearing in these are considered, $10^{-4}ms^{-2}$ results for accelerations, on the contrary $10^{-3}ms^{-2}$ for the effective forces and 10^{-1} for the ROSSBY number accordingly. Also here there is a clear tendency for the forces to balance. It is therefore allowed to set the acceleration term at zero and to study the forms of equilibrium resulting from this.

If both the tangential as well as the centripetal components of acceleration are set at zero, geostrophic equilibrium between pressure gradient and Coriolis force is obtained. It describes a straight, uniform air motion with the geostrophic wind

$$\mathbf{v}_g=-\frac{1}{\varrho f}\nabla p\times\mathbf{k} \qquad (2.6)$$

or in the natural coordinate system

$$V_g=-\frac{1}{\varrho f}\frac{\partial p}{\partial n}.$$

The geostrophic wind blows parallel to the isobars with the lower pressure values to the left (Fig 2.1). In the case of the free atmosphere above the planetary boundary layer it represents a good approximation of the true wind and can therefore be used with success for analysis and diagnosis.

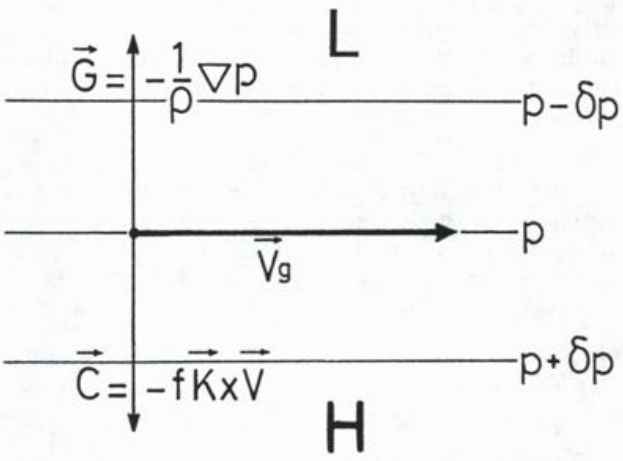

Fig. 2.1
Geostrophic wind (Northern Hemisphere)

If the tangential acceleration is set at zero as in the case of the geostrophic wind which means the motion is parallel to the isobars, but allows curved trajectories, the form of equilibrium of the gradient wind V_G is obtained with the definition equation:

$$\frac{V_G^2}{R_t}=-\frac{1}{\varrho}\frac{\partial p}{\partial n}-f V_G. \qquad (2.7)$$

As already stated in 1.2, passing through curved trajectories requires differences between pressure gradient force and Coriolis force. In the case of cyclonically curved trajectories ($R_t>0$), the gradient force must predominate, in the case of anticyclonically curved trajectories ($R_t<0$) the Coriolis force must predominate (see Fig 2.2). As, however, the Coriolis force is directly proportional to the wind speed, it results from the differences with the gradient force that the cyclonic gradient wind is weaker, in contrast the anticyclonic gradient wind is stronger than the geostrophic wind with equal pressure difference. The gradient wind consequently has the same direction as the geostrophic wind, but is sub-geostrophic in the area of cyclonic trajectories and super-geostrophic in the area of anticyclonic trajectories.

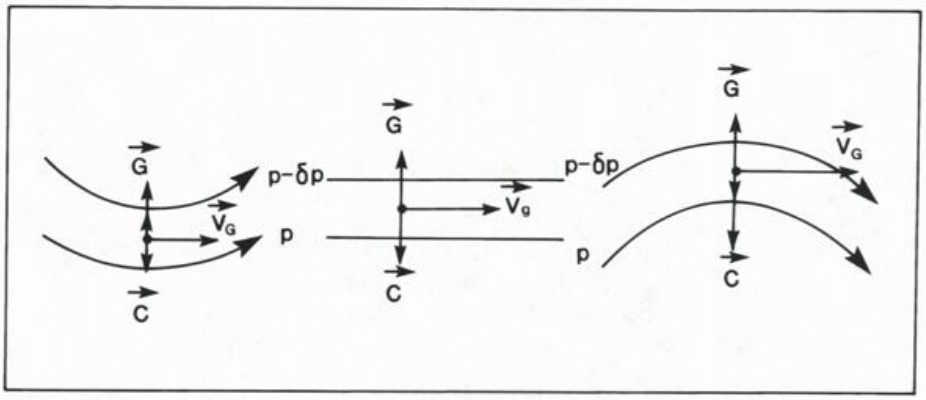

Fig. 2.2
Relation between geostrophic wind and gradient wind

Using (2.6), an arithmetical relation between the velocities of geostrophic and gradient wind

$$\frac{V_g}{V_G} = 1 + \frac{V_G}{f R_t}. \tag{2.8}$$

is obtained.

It can be seen from this that the speed differences only reach significant amounts with relatively heavy curvature. Thus a curve radius of 150 km is needed in the case of $V_g = 30 ms^{-1}$ and $f = 10^{-4} s^{-1}$, for the cyclonic gradient wind to become half as strong as the geostrophic wind. The double speed results in the area of anticyclonic trajectories with a curve radius of 1200 km.

The equation for V_G

$$V_G = -\frac{f R_t}{2} \pm \sqrt{\frac{f^2 R_t^2}{4} - \frac{R_t}{\varrho} \frac{\partial p}{\partial n}} \tag{2.9}$$

is the result from (2.7).

The positive sign before the root describes the cyclonic, the negative sign, the anticyclonic gradient wind. As the expression below the root must not be negative, the limit condition

$$|R_t| \geq \frac{4}{\varrho f^2} \left| \frac{\partial p}{\partial n} \right|$$

or (2.10)

$$|R_t| \geq \frac{4 V_g}{f}$$

results for anticyclonically curved trajectories.

With decreasing curve radius the pressure gradient therefore must also become less. In the borderline case if the root expression disappears, this becomes

$$V_G = -\frac{f R_t}{2}$$

as well as

$$V_g = -\frac{f R_t}{4} \tag{2.11}$$

and therefore

$$V_G = 2 V_g.$$

The anticyclonic gradient wind can thus achieve in extreme cases double the speed of the geostrophic wind depending on the pressure gradient. This speed was assumed in the example quoted above. The curve radius of 1200 km therefore at the same time represents the minimum value of R_t for the pressure gradient which corresponds to the assumed geostrophic wind of 30 ms^{-1}. No further balance is possible along a more heavily anticyclonically curved trajectory.

On account of the additional consideration of curved trajectories, the gradient wind describes the horizontal flow better than the geostrophic wind. In manual practice, however, no use can be made of this, as the curve radius of the trajectories is normally not known and also can only be determined with difficulty or with great expense of time. If the radius of the streamlines or isobars is used instead, serious mistakes could arise as both radii can even deviate from each other in regard to signs. The conditions for this will be discussed in the next section. Statistical evaluations have shown that gradient wind calculations, which are based on the streamline curvature, provide less accurate approximation of the true wind than the geostrophic wind (see for example KIEFER and FISCHER [7]).

The frictional force must be considered within the planetary boundary layer. It causes a slowing down of the true wind below the geostrophic speed which is especially high near the ground and fades away with increasing height. As the Coriolis force is proportional to the wind speed, it can no longer balance out the pressure gradient force in the equilibrium, so that the wind includes a component in the direction of the pressure gradient which is also at its maximum near the surface. A wind profile in the boundary layer results from this which can be ideally described by a logarithmic spiral (EKMAN spiral). The wind rotates with increasing speed to the right by sub-geostrophic winds strongly deflected to the low pressure near the ground, in order to assume geostrophic direction and speed at the upper limit of the boundary layer - at approximately a height of 1000 to 1500 m.

The frictional force is mostly given by the form

$$F = \frac{1}{\varrho} \frac{\partial \tau}{\partial z}. \tag{2.12}$$

whereby τ represents the horizontal vector of drag. The corresponding equilibrium relation then reads

$$0 = -\frac{1}{\varrho} \nabla p - f \mathbf{k} \times \mathbf{v} + \frac{1}{\varrho} \frac{\partial \tau}{\partial z}. \tag{2.13}$$

The pressure gradient force can be substituted by the geos-

trophic wind corresponding to it in the form $f\mathbf{k}\times\mathbf{v}_g$ so it follows that:

$$f\mathbf{k}\times(\mathbf{v}-\mathbf{v}_g)=\frac{1}{\varrho}\frac{\partial\tau}{\partial z}. \tag{2.14}$$

This means that the vector of the frictional force stands perpendicular to the difference vector between the true and geostrophic winds and points to the left in the Northern Hemisphere. It can be seen from Fig 2.3, which shows the equilibrium of forces for a particle in the lower part of the boundary layer, that the frictional force chiefly affects the wind in a contrary direction.

The value which the angle of deflection assumes to the isobar direction near the ground, however, varies within wide limits. It increases with higher ground roughness, greater thermal stability and decreasing geographical latitude. An angle of deflection of 30° can be assumed on average overland, whereby the ratio of V/V_g is approximately 0.5. On the contrary, over the sea the angle to the isobars is, at least in the middle and higher latitudes, very narrow (10-20°) and the wind speed reaches on average 70-80% of the geostrophic value. These relations must be remembered when analysing the pressure field at surface level.

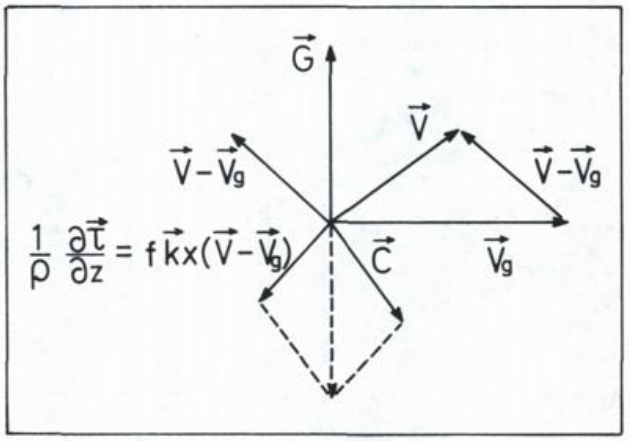

Fig. 2.3
Balance of forces with friction

2.4 Trajectories and streamlines

A trajectory describes the time-related path of an individual air particle. If we restrict ourselves to horizontal motions, the following applies for these

$$\frac{dx}{dt}=u(x,y,t);\quad \frac{dy}{dt}=v(x,y,t) \tag{2.15}$$

or in the natural system

$$\frac{ds}{dt}=V(x,y,t).$$

In contrast to this a streamline provides a "snapshot" of the motion field at a particular time. It runs tangentially to all wind vectors and can be illustrated by

$$\frac{dy}{dx}=\frac{v}{u}(x,y,t_0). \tag{2.16}$$

By introducing the natural coordinate system in 1.2, the following resulted for trajectory curvature K_t

$$K_t=\frac{d\beta}{ds},$$

whereby $d\beta$ reflects the change of the wind direction over the distance ds along the horizontal trajectory. In the case of the time-related change

$$\frac{d\beta}{dt}=\frac{d\beta}{ds}\frac{ds}{dt}=VK_t \tag{2.17}$$

is therefore obtained.

On the other hand $d\beta/dt$ can be split up into

$$\frac{d\beta}{dt}=\frac{d\beta}{dt}+v\cdot\nabla\beta$$

or (2.18)

$$\frac{d\beta}{dt}=\frac{d\beta}{dt}+V\frac{d\beta}{ds}.$$

$d\beta/dt$ is the local change in direction while $d\beta/ds$ describes the horizontal variation of β for a fixed time and therefore exactly corresponds to the curvature K_s of streamlines. In consideration of this identity, the equation first quoted by BLATON

$$\frac{d\beta}{dt}=V(K_t-K_s) \tag{2.19}$$

results from (2.17) and (2.18).

In a stationary field local change in the wind direction disappears so that $K_t = K_s$ results. When stationary, streamlines and trajectories are identical. When not stationary, the curvature of the trajectories can be calculated from streamlines and isotach analyses taking into consideration local change in direction.

The Blaton equation will next be used in order to study the relation between trajectories and streamlines in moving pressure systems. In doing so systems with closed isobars will be considered initially as they are characteristic of the surface field.

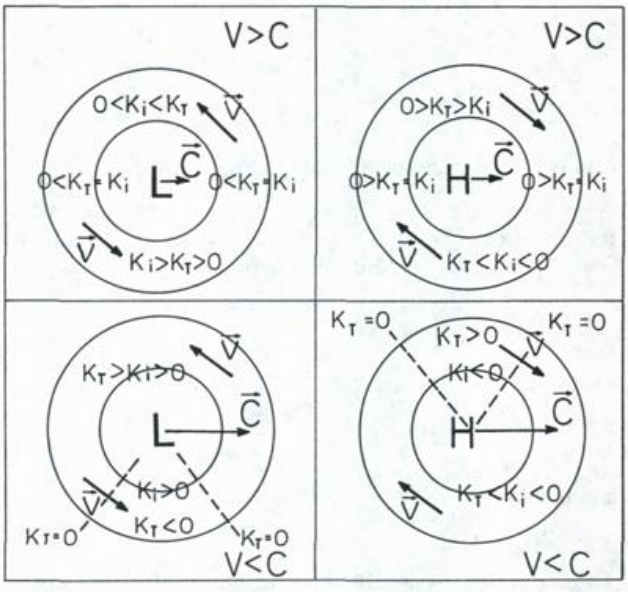

Fig. 2.4
Comparison of isobar and trajectory curvature

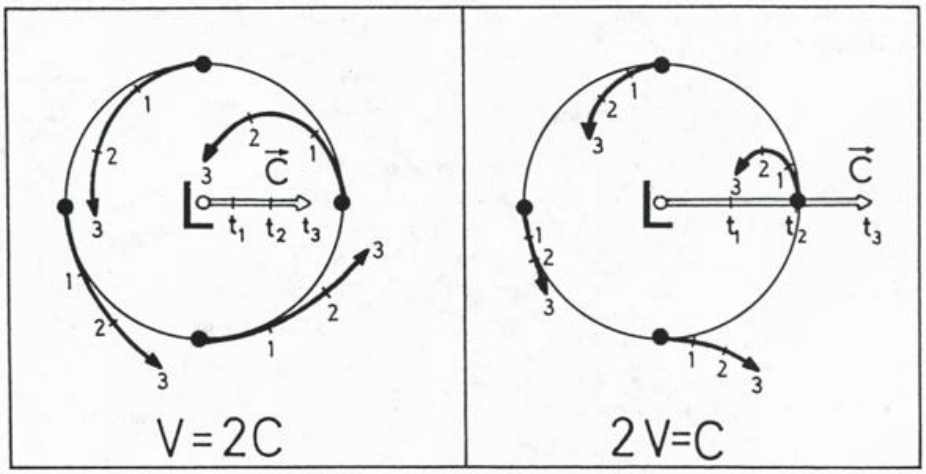

Fig 2.5
Trajectories in the area of a cyclone with V>c and V<c. According to HOLTON [3].

c is the speed vector of the moving streamline field. If the form of this field does not change in respect to time, the local wind change is caused solely by the movement of the system:

$$\frac{d\beta}{dt} = -c \cdot \nabla\beta = -c \cos\gamma \frac{d\beta}{ds},$$

whereby γ means the angle between the streamlines and the direction of movement of the system observed.

Using (2.19)

$$V(K_t - K_s) = -c \cos\gamma \frac{d\beta}{ds}$$

and (2.20)

$$K_t = \frac{V - c\cos\gamma}{V} K_s$$

are obtained.

Inside a balanced flow the streamline curvature is identical with the isobar curvature K_i.

Clearly the relation between trajectory and isobar curvature depends on the ratio of V to c. Two cases must be distinguished accordingly:

1 V>c: The wind speed is greater than the speed of movement. As Fig 2.4 shows K_t and K_i then have the same sign. However, the trajectory curvature is greater than the isobar curvature left of the path in the case of moving cyclones and right in the case of moving anticyclones as well as less on the opposite fringes (see Fig 2.5). $K_t = K_i$ along the path of the system.

2 c>V: The speed of movement is greater than the wind speed. In this case $K_t = 0$ on the border of a sector, determined by $\cos\gamma = \frac{V}{c}$.

Within this sector the trajectory has an opposite curvature to the isobars. In the case of a quickly moving cyclone this can be expected on the right of the path, in the case of an anticyclone on the fringe left of the path (see Fig 2.5).

If gradient wind equilibrium is assumed, the different trajectory curvature has consequences for the wind distribution in moving pressure systems. In the case of cyclones the strongest sub-geostrophic winds can be expected on the fringe left of the path while on the opposite side the winds where c>V can even be supergeostrophic. Conversely, in the case of anticyclones, the winds on the fringe right of the path are at the strongest super-geostrophic while on the another side the winds where c>V are below the geostrophic value. The limit (2.10) also applies to the centre and the right fringe of anti-cyclones so that the pressure gradient there must not exceed certain limits.

In contrast to the surface field, wave-shaped streamlines predominate in higher altitudes. As the phase speed of these waves is always less than the wind speed, K_t and K_s have the same sign everywhere. Again assuming gradient wind equilibrium, this means that winds in the area of troughs must be more or less strongly sub-geostrophic, in the area of ridges on the contrary super-geostrophic. However, the trajectory curvature in the area of the trough and ridge axes is less than the streamline curvature. This must be remembered when using the gradient wind relation qualitatively. At the turning point of streamlines the trajectory curvature also becomes zero. Geostrophic winds can be used there for initial approximate calculations.

In the case of ridges of the upper current, again the boundary condition betweeen anticyclonic trajectory curvature and pressure gradient applies. It is of importance if the particles which pass through a ridge with critical curvature reach greater speed as a result of any kind of process. They can then no longer follow the previous trajectory and shoot away over the high pressure ridge. As a result greater adjustments can be introduced in the wind and pressure field (see 13.9.5).

Interesting relations result for the amplitudes and wave lengths of the trajectories within these kinds of waves. For simplification it is assumed that the sine-shaped streamlines lie over a zonal basic flow U and the wave resulting from this moves without changing amplitude with time-related constant speed c in the direction of the basic flow. In this case

$$\frac{dy}{dx} = \frac{v}{U} = \frac{v_0}{U} \cos\left[\frac{2\pi}{L_s}(x - ct)\right], \qquad (2.21)$$

applies for any particular streamline, which with constant v_0, U and c can be integrated to

$$y = \frac{v_0}{2\pi}\frac{L_s}{U}\sin\left[\frac{2\pi}{L_s}(x-ct)\right] + k. \qquad (2.22)$$

Integration-constant k determines the position of the individual streamlines in the field. Corresponding to Fig 2.6, k = 0 for the streamline which pivots about the x-axis.

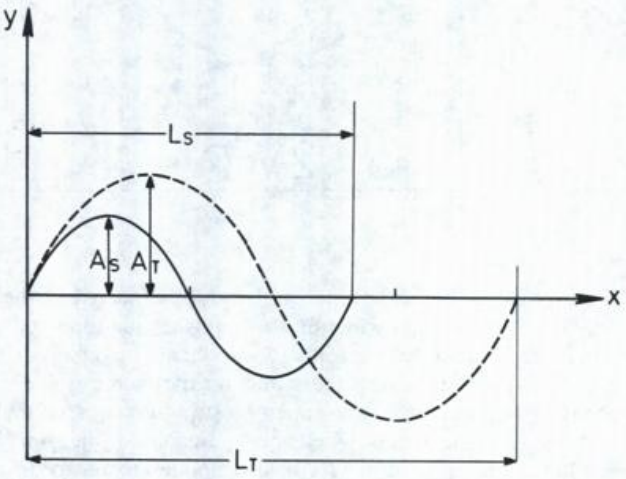

Fig. 2.6
Sine-shaped streamline (solid line) and associated trajectory (broken line) with U>c>0

If the trajectory which begins at the turning point of the streamlines with $x_0 = y_0 = 0$ is now determined,

$$x = Ut,$$

$$y = \frac{v_0 L_s}{2\pi(U-c)}\sin\left[\frac{2\pi}{L_s}\left(1-\frac{c}{U}\right)x\right] \qquad (2.23)$$

results from the integration of (2.15) in consideration of (2.21), whereby t has been replaced by x/U in the second equation.

It can be seen from this that the trajectory is also sine-shaped but differs in amplitude and wavelength from the streamline.

$$\frac{A_t}{A_s} = \frac{L_t}{L_s} = \frac{U}{U-c} \qquad (2.24)$$

results from comparing (2.22) and (2.23) for the ratio of both amplitudes and wavelengths.

In the case of a wave moving progressively in the direction of the basic flow (U>c>0), amplitude and wavelength of the trajectory are therefore greater than those of the streamline, on the contrary less in the case of a retrogressive wave (U>0>c). In the case of stationary waves, streamlines and trajectories are identical.

In the following sections relative motions within a moving coordinate system are frequently considered, whereby the relative system is coupled to a moving cyclone or a wave of the upper air current. If - as assumed above - the shape of the moving streamline field does not change in respect to time, the motion remains stationary within the relative system. In this case the relative streamlines can be constructed very easily by subtracting the movement field graphically from the normal streamline field.

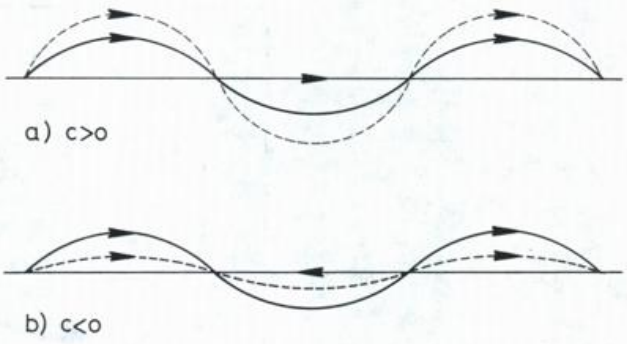

Fig. 2.7
Relation between streamlines (solid lines) and relative streamlines (broken lines) with c>0(a) and c<0(b)

In Fig 2.7 this process is illustrated for a moving wave, once for motion of the wave in the direction of the basic flow, once in the opposite direction. It can be recognized that in the first case the relative streamlines have a larger, in the second case a smaller amplitude than the streamlines, while the wavelengths of both lines are the same.

This fact can also be shown in equations. While

$$\left(\frac{dy}{dx}\right)_s = \frac{v}{U}$$

applies for the streamline,

$$\left(\frac{dy}{dx}\right)_r = \frac{v}{U-c}$$

is obtained for the relative streamline under the conditions described.

$$\left(\frac{dy}{dx}\right)_r = \frac{U}{U-c}\left(\frac{dy}{dx}\right)_s \qquad (2.25)$$

results from the combination of both equations.

As U and c should be independent from x, this can be integrated to

$$y_r = \frac{U}{U-c}y_s$$

and as the amplitudes represent the extreme value of the ordinate,

$$\frac{A_r}{A_s} = \frac{U}{U-c}$$

or (2.26)

$$A_r = \frac{U}{U-c}A_s$$

also applies.

The same relation also results therefore as for the amplitudes of the trajectories. The wave length of the relative streamlines is on the contrary identical with that of the normal streamlines since the relative system moves together with the wave.

2.5 Pressure as vertical coordinate

It is known that the pressure distribution on defined level surfaces is not analysed on charts for the free atmosphere but conversely the height or geopotential distribution of se-

lected pressure surfaces is represented. These analyses are called absolute topographies; the isolines of equal geopotential are named isohypses on account of the numerical similarity of z and ϕ.

For this method it is necessary to change the equation of motion and the equation for the geostrophic wind from the normal z-system into a system with the pressure as vertical coordinate. For this purpose the general equation

$$\nabla_\psi s = \nabla s + \frac{\partial s}{\partial z} \nabla_\psi z \tag{2.27}$$

is used.

Here $-\nabla s$ is the normal horizontal gradient of a scalar variable s, $-\nabla_\psi$ s the horizontal gradient of s determined on the horizontal projection of a surface Ψ =const. and $-\nabla_\psi$ z the horizontal gradient of height z of this surface.

With Ψ = p and s = p we obtain ∇_p p=0. Using the hydrostatic equation and the definition equation of the geopotential

$$\nabla p = g\varrho \nabla_p z = \varrho \nabla_p \Phi \tag{2.28}$$

follows in this case.

The equation of motion (1.7) therefore assumes the form

$$\frac{d\mathbf{v}}{dt} = -\nabla_p \Phi - f\mathbf{k} \times \mathbf{v} \tag{2.29}$$

and for the geostrophic wind

$$\mathbf{v}_g = -\frac{1}{f} \nabla_p \Phi \times \mathbf{k} \tag{2.30}$$

results.

In contrast to the z-system, the considerably height variable density no longer appears in these equations. A nomogram with the help of which the potential gradient can be determined from the wind observations in accordance with (2.30) can therefore be used universally for all pressure surfaces. This is one of the many advantages which the p-system offers in synoptic practice. In addition, however, for theoretical investigations it is also in most cases superior to the z-system.

For the geopotential difference between two pressure surfaces (p_o,p_1), which is also described as layer thickness or relative topography, a relation is obtained from the hydrostatic equation. Integration of (2.4) produces

$$D \equiv \Phi_1 - \Phi_0 = R_d \int_{p_1}^{p_0} T_v \, d \ln p \tag{2.31}$$

as well as for averaging the virtual temperature

$$D = R_d \ln\left(\frac{p_0}{p_1}\right) \bar{T}_v . \tag{2.32}$$

D is directly proportional to the virtual mean temperature. The representation of a relative topography therefore directly reflects the pattern of the mean temperature distribution in which the zones of steep temperature gradients, the thermal frontal zones, can be recognised. For this reason the relative topographies, which include the lower troposphere (normally the RT 500/1000 hPa), represent a valuable aid in the analysis of surface fronts.

2.6 Vertical change of the geostrophic wind

If it is assumed that wind and pressure fields are found nearly in geostrophic equilibrium above the planetary boundary layer, the vertical change of the wind vector is chiefly determined by change in the geostrophic wind.

For the vector difference

$$\Delta \mathbf{v}_g = \mathbf{v}_{g1} - v_{g0}$$

between pressure surfaces p_0 and p_1

$$\Delta \mathbf{v}_g = -\frac{1}{f} \nabla(\Phi_1 - \Phi_0) \times \mathbf{k}$$

or

$$\Delta \mathbf{v}_g = -\frac{1}{f} \nabla D \times \mathbf{k} \tag{2.33}$$

is obtained from the definition equation for the geostrophic wind and using (2.32)

$$\Delta \mathbf{v}_g = -\frac{R_d}{f} \ln\left(\frac{p_0}{p_1}\right) \nabla \bar{T}_v \times \mathbf{k}. \tag{2.34}$$

The difference vector therefore lies parallel to the relative isohypses with the lower values to the left (see Fig 2.8). It therefore also runs parallel to the isotherms of the mean temperature with the colder air to the left. On account of this relation with the temperature field $\Delta \mathbf{v}_g$ is also frequently described as "thermal wind" ($\mathbf{v}_T$).

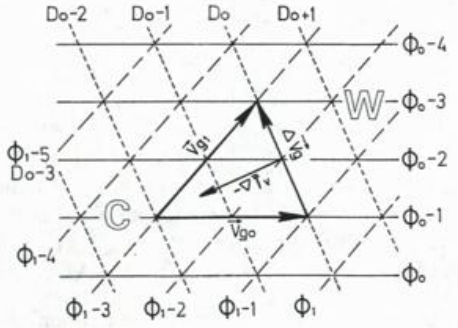

Fig. 2.8
Relation between $\Delta \mathbf{v}_g$ and virtual mean temperature

The "thermal wind equation" for the vertical shear of the geostrophic wind

$$\frac{\partial \mathbf{v}_g}{\partial z} = -\frac{g}{fT_v} \nabla_p T_v \times \mathbf{k} \tag{2.35}$$

results from (2.34) and (2.32) after the limit is exceeded.

The various types of vertical wind change which result from the two equations are shown diagramatically in Fig 2.9 and can be finally characterised in short:

a) If the isotherms run parallel to the isohypses and the colder air lies under the lower geopotential, the geostrophic wind increases with height without changing direction.

b) If with parallel lines the warmer air lies under the lower geopotential, the geostrophic wind decreases with height, whereby a change in direction of 180° is then possible.

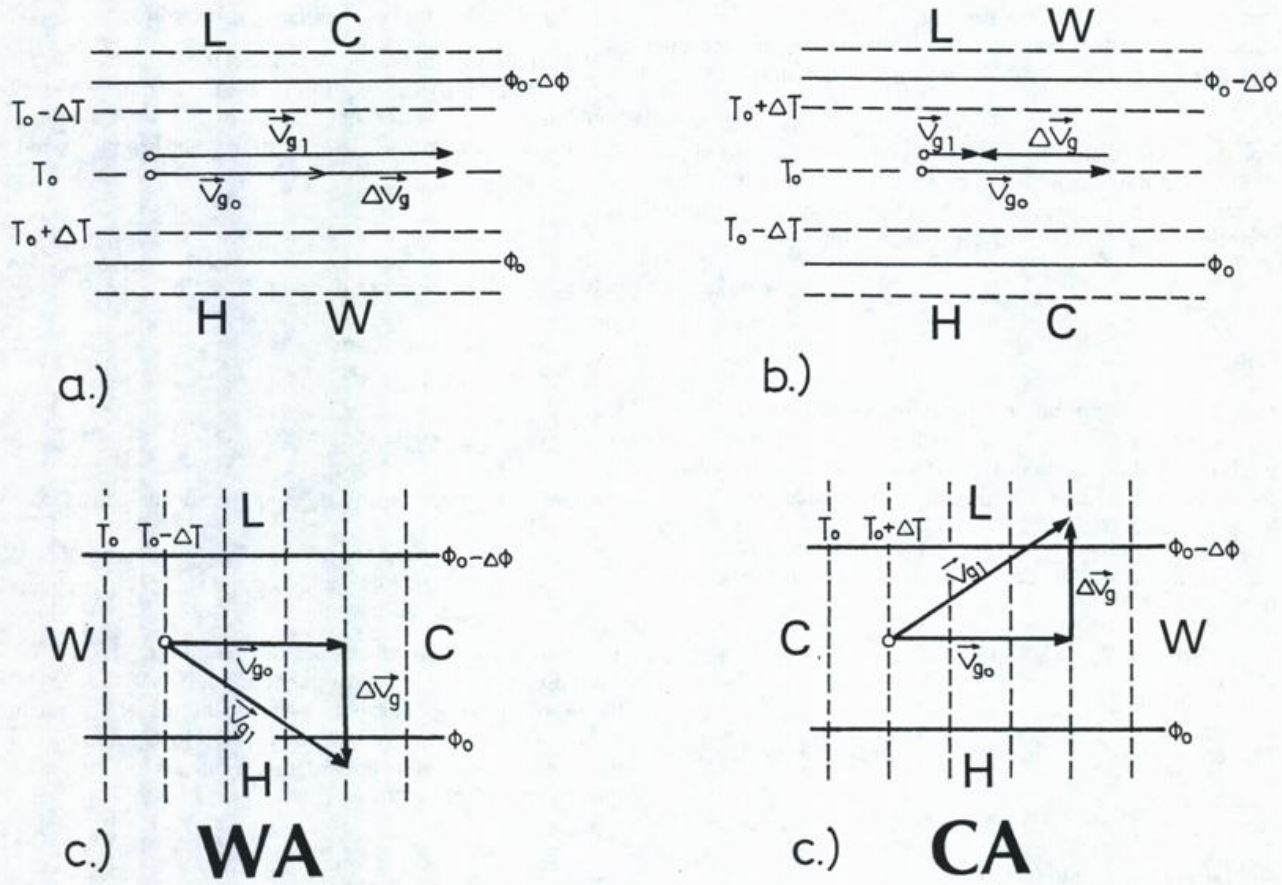

Fig. 2.9
Types of vertical wind change

c) If isohypses and isotherms intersect, a change in direction of the geostrophic wind occurs with height. Simultaneously an advection of air with different temperature occurs with the wind. The sketch shows that veering is associated with warm air advection (WA) and backing is associated with cold air advection (CA).

d) If the isobaric gradient of the virtual temperature disappears, the geostrophic wind remains constant in height.

Cases a) to c) characterise baroclinic, Case d) barotropic stratification of the atmosphere.

2.7 Temperature advection and local temperature change

The horizontal temperature advection which appeared in Case c) is defined by

$$A_T = -\mathbf{v}\cdot\nabla T$$

or in the p-system (2.36)

$$A_T = -\mathbf{v}\cdot\nabla_p T.$$

Knowledge of this is very important for diagnostic and prediction purposes. It is one of the three components by which local temperature change $\partial T/\partial t$ is determined.

From the first law of thermodynamics follows, with differentiation according to time

$$\frac{dQ}{dt} = c_p\frac{dT}{dt} - \alpha\frac{dp}{dt}.$$

Splitting up of dp/dt using the hydrostatic equation results in

$$c_p\frac{dT}{dt} = \frac{dQ}{dt} + \alpha\frac{\partial p}{\partial t} + \alpha\,\mathbf{v}\cdot\nabla p - g\,w.$$

Calculations have shown that the influence of the two right-hand middle terms on temperature change is slight.

$$\frac{\partial T}{\partial t} = -\mathbf{v}\cdot\nabla T - (\gamma_t - \gamma)\,w + \frac{1}{c_P}\frac{dQ}{dt} \qquad (2.37)$$

can therefore be written with good approximation.

An analogous relation applies for the p-system. Local temperature increases occur corresponding to (2.37) as a result of

a) Advection of warmer air
b) Descending motion in the case of stable stratification and/or
c) Diabatic heat gain.

Conversely local temperature decreases as a result of

a) Advection of colder air
b) Ascending motion in the case of stable stratification and/or
c) Diabatic heat loss.

In the case of vertical motions with condensation, the release of latent heat must be considered. This can be done either by introduction of γ_f instead of γ_t or as a result of corresponding changes in the diabatic term.

While the last two terms in (2.37) can routinely be recorded only with difficulty, the influence of temperature

advection can be determined with sufficient accuracy. Under the assumption that advection is mainly controlled by the geostrophic wind,

$$A_T \approx -\mathbf{v}_g \cdot \nabla_p T,$$

applies (in the p-system) so that sign and amount of advection can be read by superposing the geopotential and temperature fields. If the isohypses run in the direction of the geostrophic wind from low to high temperatures, this is cold air advection ($A_T<0$), conversely if they run from high to low, warm air advection prevails ($A_T>0$). The amount of temperature advection can be estimated qualitatively from the density of the intersect points between isohypses and isotherms.

As well as temperature advection on the individual pressure surfaces, geostrophic advection of the average temperature is frequently determined between selected pressure surfaces e.g. between 500 and 1000 hPa. In doing so it is assumed that $\mathbf{v}_g$ changes linearly with height. As Fig 2.10 demonstrates all wind vectors within the layer in this case have the same normal component regarding the relative isohypses as the middle wind $\bar{\mathbf{v}}_g$ and

$$\bar{A}_T \approx -\bar{\mathbf{v}}_g \cdot \nabla \bar{T}_v$$

applies.

Accordingly the advection can be calculated by superposing RT 500/1000 hPa on the surface chart. The surface isobars are followed and marked, in each case according to whether they run from low to high or from high to low values of RT, cold air advection or warm air advection by suitable colours or symbols.

Assuming geostrophic equilibrium, statements about the temperature advection in the area concerned can also be obtained from the wind reports of a single aerological station. For this purpose the wind values of the height or pressure levels following each other are entered in a polar diagram (see Fig 2.11).

The curve which joins the tips of the wind vectors with each other is the hodograph. The change vector $\partial \mathbf{v}/\partial z$ forms the tangent to this curve. Assuming that

$$\frac{\partial \mathbf{v}}{\partial z} \approx \frac{\partial \mathbf{v}_g}{\partial z}$$

the direction of the isotherms at the various levels is immediately obtained from the direction of the tangent. Again the sign of temperature advection can be read off in conjunction with the wind direction.

In the sketch in 2.11 warm air advection is indicated at all levels.

This method is, however, also suitable for determining temperature advection quantitatively. Assuming $T \approx T_v$

$$\nabla_p T = -\frac{f}{g} T\mathbf{k} \times \frac{\partial \mathbf{v}_g}{\partial z},$$

is obtained from (2.35).

from which

$$A_T = \frac{f}{g} T\mathbf{v}_g \cdot \left(\mathbf{k} \times \frac{\partial \mathbf{v}_g}{\partial z}\right)$$

or

$$A_T = -\frac{f}{g} T\mathbf{k} \cdot \left(\mathbf{v}_g \times \frac{\partial \mathbf{v}_g}{\partial z}\right) \qquad (2.38)$$

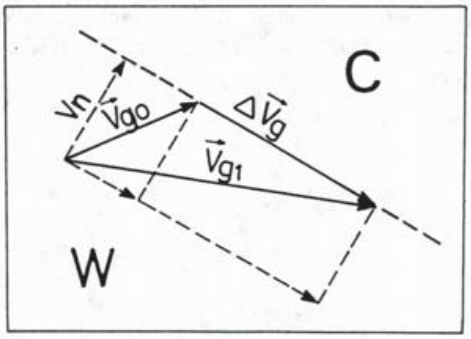

Fig. 2.10
(See text)

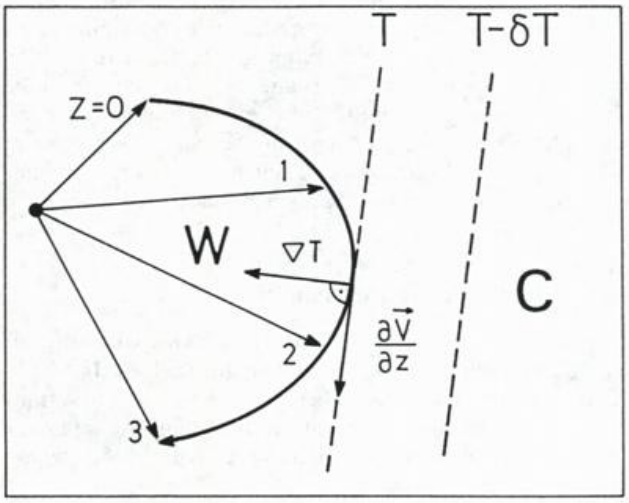

Fig. 2.11
Hodograph

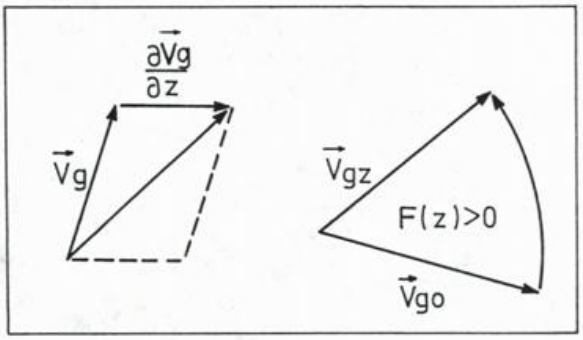

Fig. 2.12
(See text)

follows for the geostrophically approximated temperature advection A_T.

The triple product $\mathbf{k} \cdot \left(\mathbf{v}_g \times \frac{\partial \mathbf{v}_g}{\partial z}\right)$ is equal in sum to the area of the parallelogram which is produced by vectors $\mathbf{v}_g$ and $\partial \mathbf{v}_g/\partial z$ and accordingly is twice as great as the triangular area produced by the two vectors in the polar diagram (see Fig 2.12).

Therefore the advective temperature change is proportional to the area over which the wind vector propagates over the hodograph curve. If

$$F(z) = \frac{1}{2}\mathbf{k} \cdot \int_0^z \mathbf{v}_g \times d\mathbf{v}_g$$

is defined, F(z) is the area which is embraced by $\mathbf{v}_g(0)$, $\mathbf{v}_g(z)$ and the hodograph. It is positive if $\mathbf{v}_g$ rotates to the left with height.

In this case

$$\frac{dF}{dz} = \frac{1}{2}\,\mathbf{k}\cdot\left(\mathbf{v}_g \times \frac{\partial \mathbf{v}_g}{\partial z}\right)$$

and (2.40)

$$A_T = -2\,\frac{f}{g}\,T\,\frac{dF}{dz}$$

apply.

Apart from this evaluation, the hodograph is also of great help when analysing the temperature field. Assuming geostrophic equilibrium, the direction of the isotherms at the various levels can be read - as already remarked - from the hodograph curve. In addition the temperature gradient can be calculated from the length of the curved sections. In cases of doubt hydrostatically reliable and vertically uniform isothermic analysis is possible as a result.

2.8 Changes in vertical stability

Horizontal temperature advection is in many cases the determining factor for local temperature changes. If advection is different at various heights and as a result various temperature changes occur, the vertical temperature gradient must also change. This is however synonymous with a change in vertical stability.

A relation for the local time-related change in the vertical temperature gradient

$$\frac{\partial \gamma}{\partial t} = -\frac{\partial A_T}{\partial z} + (\gamma_t - \gamma)\,\frac{\partial w}{\partial z} - w\,\frac{\partial \gamma}{\partial z} - \frac{1}{c_p}\,\frac{\partial}{\partial z}\left(\frac{\partial Q}{\partial t}\right) \qquad (2.41)$$

is obtained immediately from (2.37) with partial differentiation in accordance with z.

As well as through vertically varying temperature advection and vertical advection of γ, stability changes occur if the vertical motions or diabatic heat fluxes have a vertical gradient.

As a result of vertically varying advection, stabilization occurs in the case of

a) WA, increasing with height
b) CA, decreasing with height
c) WA above CA

and destabilization in the case of

a) WA, decreasing with height
b) CA, increasing with height
c) CA above WA

(WA is warm air advection, CA is cold air advection).

The geostrophic part of temperature advection can be easily estimated if a hodograph curve is available. As A_T is proportional to the area within the hodograph curve, the changes in area expansion with increasing height (d^2F/dz^2)

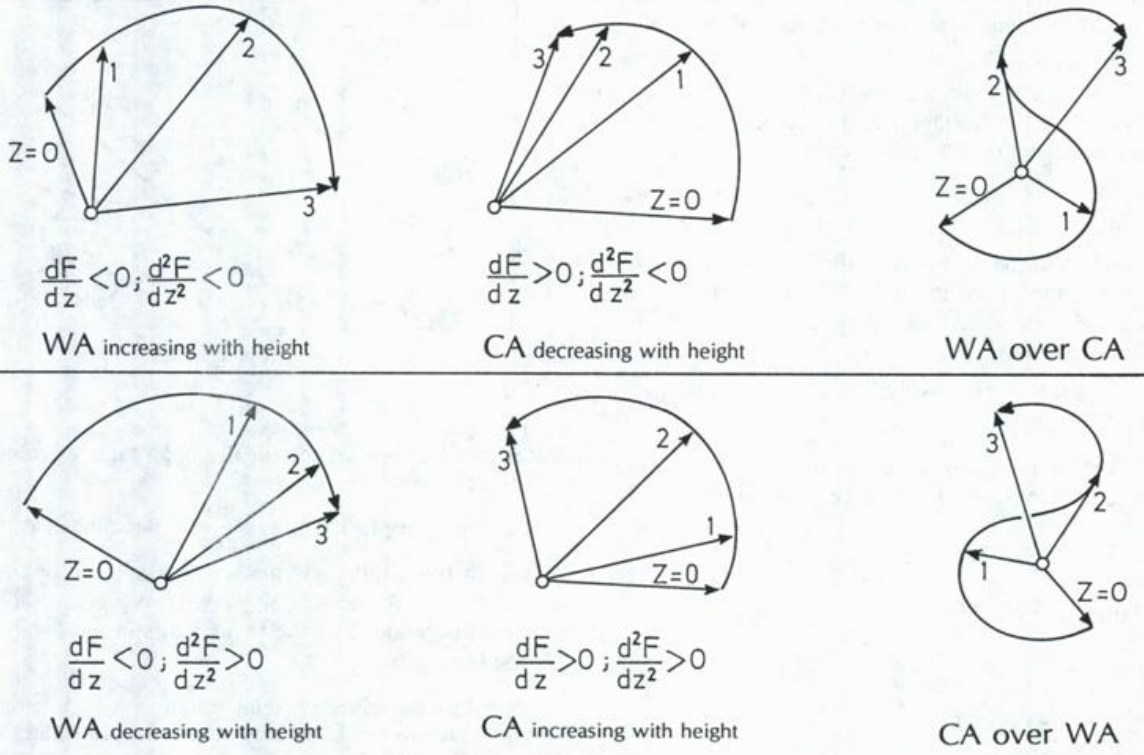

Fig. 2.13
Hodographic curves in the case of advective change in stability
Top: Stabilizing tendency Bottom: Destablizing tendency

are a measure of changes in stability which result from $(-\partial A_T/\partial z)$. Some cases are shown in Fig 2.13.

However, it is important to point out that changes in stability which result from vertically varying advection go back for the most part simply to horizontal advection of an air mass with a corresponding change in stability. It can be seen that if A_T is differentiated vertically and at the same time the horizontal wind vector is split into $\mathbf{v}_g$ and an ageostrophic part $\mathbf{v}^*$ (see 2.10):

$$-\frac{\partial A_T}{\partial z} = -\frac{\partial}{dz}(-\mathbf{v}_g \cdot \nabla T - \mathbf{v}^* \cdot \nabla T)$$
$$= -\mathbf{v}_g \cdot \nabla\left(-\frac{\partial T}{\partial z}\right) - \mathbf{v}^* \cdot \nabla\left(-\frac{\partial T}{\partial z}\right)$$
$$+\frac{\partial \mathbf{v}_g}{\partial z} \cdot \nabla T + \frac{\partial \mathbf{v}^*}{\partial z} \cdot \nabla T.$$

As $\frac{\partial \mathbf{v}_g}{\partial z} \cdot \nabla T$ in accordance with (2.35) disappears,

$$-\frac{\partial A_T}{\partial z} = -\mathbf{v} \cdot \nabla \gamma + \frac{\partial \mathbf{v}^*}{\partial z} \cdot \nabla T \qquad (2.42)$$

results.

The above statement is entirely true for geostrophoic conditions. Additional destabilizing or stabilizing effects occur only if the ageostrophic wind part has vertical differences in the direction of the temperature gradient.

In regard to the influence of the vertical motions it can be assumed that with $(\gamma_t - \gamma) > 0$ the stratification is dry stable. Destabilizing can occur if with $\partial w/\partial z > 0$ the air column is stretched vertically. If a distribution with disappearing vertical motions near to the ground as well as at greater heights and its maximum somewhere in the middle troposphere is assumed, this applies to the area below the strongest ascent or above the strongest descent. Above the level of the strongest ascent or below the level of the strongest descent, conversely, a further increase in stability of the given stable stratification occurs as a result of vertical contraction.

In addition destabilizing occurs if near the surface the strongest heat gain or at a height the strongest heat loss takes place. The first occurs during diurnal heating of the air from the earth's surface, the second, for example, during radiational cooling from cloud surfaces. A very great possibility of destabilizing exists moreover if in the case of ascending motion, condensation occurs and heat is released in the lower layers, but, however, not above it. This is the deciding factor in the triggering of "potential instability" defined in 2.2. With regard to stabilization by vertically varying diabatic heat transfer on the other hand, this occurs for example by nocturnal cooling of the earth from the ground or by evaporation of rain below clouds.

2.9 Vertical structure of pressure systems

In the following some relations defining the structure of the pressure systems will be derived. Here on the one hand the tilt of the vertical axis and on the other the change in intensity with height are of interest. Consideration is carried out in the p-system.

For the centre of a depression the following applies if z represents the height of a pressure surface:

$$\frac{\partial z}{\partial x} = \frac{\partial z}{\partial y} = 0$$

and also

$$\frac{\partial^2 z}{\partial x^2} > 0, \quad \frac{\partial^2 z}{\partial y^2} > 0.$$

As these conditions are also valid along the axis inclined in the x-direction (see Fig 2.14),

$$\delta\left(\frac{\partial z}{\partial x}\right) = 0$$

or

$$\frac{\partial}{\partial x}\left(\frac{\partial z}{\partial x}\right)\delta x + \frac{\partial}{\partial p}\left(\frac{\partial z}{\partial x}\right)\delta p = 0$$

can be written.

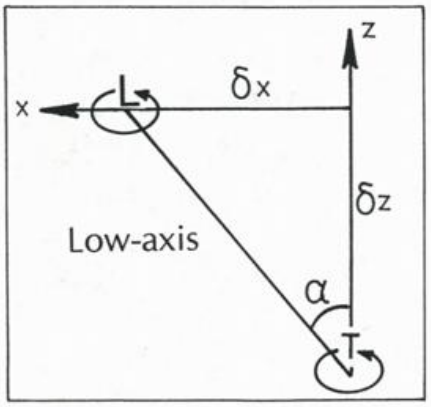

Fig. 2.14
Tilt of axis of a low pressure system

For the angle of inclination α to the vertical

$$\mathrm{tg}\,\alpha \equiv \frac{\delta x}{\delta z} = -g\varrho\frac{\delta x}{\delta p} = g\varrho\frac{\frac{\partial}{\partial x}\left(\frac{\partial z}{\partial p}\right)}{\partial^2 z/\partial x^2} \qquad (2.43)$$

results from this and, since

$$\frac{\partial z}{\partial p} = -\frac{1}{g\varrho},$$

$$\mathrm{tg}\,\alpha = g\varrho\,\frac{\partial\left(-\frac{1}{g\varrho}\right)/\partial x}{\partial^2 z/\partial x^2}$$

as well as

$$\mathrm{tg}\,\alpha = \frac{1}{\varrho}\frac{\partial\varrho/\partial x}{\partial^2 z/\partial x^2}. \qquad (2.44)$$

Where p=const.

$$T\left(\frac{\partial\varrho}{\partial x}\right)_p + \varrho\left(\frac{\partial T}{\partial x}\right)_p = 0$$

results from the equation of state and for

$$\frac{1}{\varrho}\left(\frac{\partial \varrho}{\partial x}\right)_p = -\frac{1}{T}\left(\frac{\partial T}{\partial x}\right)_p.$$

Using this, the following then results

$$\mathrm{tg}\alpha = \frac{1}{T}\frac{(-\partial T/\partial x)_p}{\partial^2 z/\partial x^2}. \qquad (2.45)$$

With $\alpha>0$ and $\partial^2 z/\partial x^2>0$ the term $(-\partial T/\partial x)_p$ must also be positive which signifies a temperature decrease in the x-direction. This means that the vertical axis of a low tends to run to the coldest air. For a high on the other hand $\partial^2 z/\partial x^2<0$ applies so that the axis tends to run towards the warmest air (see Fig 2.15a). The tendency here is all the greater the the greater the temperature gradient, all the less the greater the curvature of the height profile of the pressure surface concerned. If $(-\partial T/\partial x)_p = 0$ the axis is vertical. This is the case on the one hand with barotropy, the case on the other hand if the pressure centre coincides with a temperature extreme.

Change in intensity of a pressure system with height can be described by the vertical variation of the pressure surface inclination

$$\frac{\partial}{\partial z}\left(\frac{\partial z}{\partial x}\right)$$

which is directly proportional to the strength of the geostrophic equilibrium wind in accordance with (2.30). As

$$\frac{\partial}{\partial z} = -g\varrho\frac{\partial}{\partial p}$$

the following is obtained for

$$\frac{\partial}{\partial z}\left(\frac{\partial z}{\partial x}\right) = -g\varrho\frac{\partial}{\partial p}\left(\frac{\partial z}{\partial x}\right)$$

$$= -g\varrho\frac{\partial}{\partial x}\left(\frac{\partial z}{\partial p}\right)$$

$$= -\frac{1}{\varrho}\left(\frac{\partial \varrho}{\partial x}\right)_p$$

so that with (2.45)

$$\frac{\partial}{\partial z}\left(\frac{\partial z}{\partial x}\right) = \frac{1}{T}\left(\frac{\partial T}{\partial x}\right)_p \qquad (2.46)$$

results.

Applied to a cold low with a vertical axis this means that its intensity increases with height as $(\partial T/\partial x)_p$ is generally positive outside the centre (see Fig 2.15b). A cold low is therefore a vertically deep system. Similar considerations apply for a warm high pressure area, the intensity of which also increases with height. Flat pressure systems are on the contrary warm cyclones and cold anticyclones. In these cases a decrease in intensity results from (2.46) with height. If in such a case the temperature field maintains its orientation in the vertical plane, a sign change of the geopotential gradient occurs at a certain height. Then a high lies at a height above the warm surface low, but a low above the cold surface high.

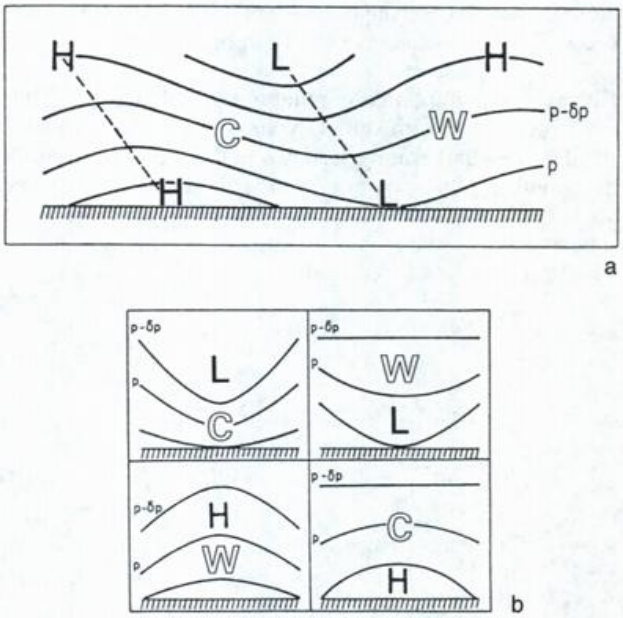

Fig. 2.15
Vertical tilt of axis (a) and change in intensity (b) of pressure systems depending on the temperature

2.10 Ageostrophic wind components

As already mentioned the geostrophic equilibrium above the planetary boundary layer is on average such that the geostrophic wind can be used as an aid for analysing the topographies. The differences in equilibrium, the so-called ageostrophic wind components, are therefore normally relatively minor. However, they cannot be neglected as even these are of decisive importance in the synoptic processes.

A relation for the ageostrophic wind component

$$\mathbf{v}^* = \mathbf{v} - \mathbf{v}_g \qquad (2.47)$$

is obtained if as already executed once, the pressure gradient force in the horizontal equation of motion is substituted by the geostrophic wind in the form $f\,\mathbf{v}_g \times \mathbf{k}$.

In this case

$$\frac{d\mathbf{v}}{dt} = f(\mathbf{v} - \mathbf{v}_g)\times\mathbf{k} = f\,\mathbf{v}^*\times\mathbf{k} \qquad (2.48)$$

results.

This relation tells us that the acceleration vector is perpendicular to the vector of the ageostrophic component and points to the right. It will be used in the following in order to describe - based on acceleration - the various forms of the ageostrophic wind part.

Here it is assumed that due to the tendency of the atmosphere to balance out, not only the ageostrophic wind part itself but also its time-related change is minimal. In the case of oscillations around the balance condition, this applies at least for the time mean. In the first approximation the actual acceleration $d\mathbf{v}/dt$ which receives a particle can in this case be replaced by the change in the geos-

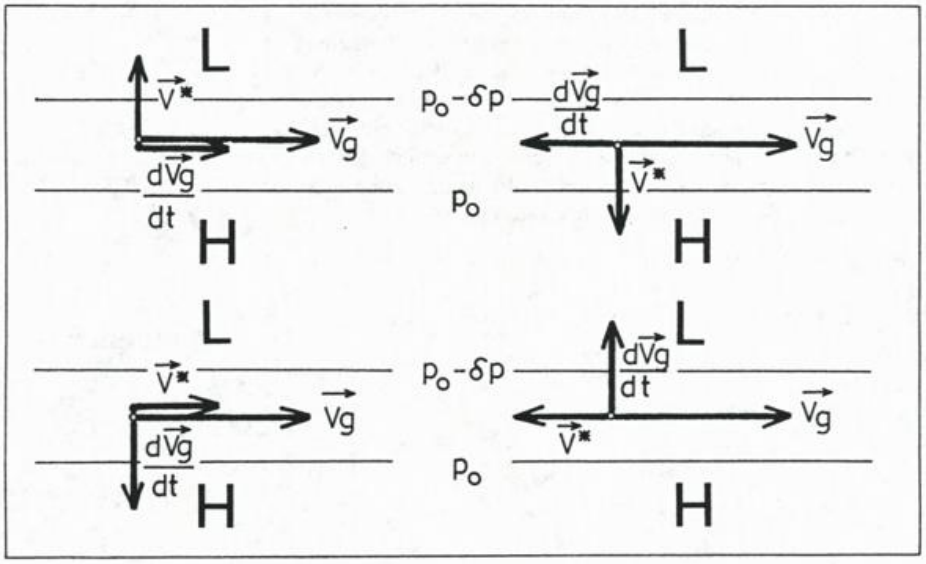

Fig. 2.16
Ageostrophic wind component and acceleration

trophic wind $d\mathbf{v}_g/dt$ to which it is subject along its trajectory:

$$\frac{d\mathbf{v}}{dt} \approx \frac{d\mathbf{v}_g}{dt} = f\,\mathbf{v}^* \times \mathbf{k}$$

and

$$\mathbf{v}^* = \frac{1}{f}\,\mathbf{k} \times \frac{d\mathbf{v}_g}{dt}. \qquad (2.49)$$

Therefore there is a relation at the same time with the pressure field. In addition, if the split in the tangential and centripetal acceleration part is considered, it generally results from (2.49) that changes in velocity of the geostrophic wind must be associated with ageostrophic components across the wind direction, changes in the direction of the geostrophic wind on the other hand with ageostrophic components parallel to the wind direction. With velocity increase an ageostrophic component is linked to low pressure, with velocity decrease to high pressure. In the case of change in direction to the right $\mathbf{v}^*$ points in the wind direction which means super-geostrophic winds, in the case of a change of direction to the left against the wind direction, due to which sub-geostrophic winds result (see Fig 2.16).

In accordance with

$$\frac{d\mathbf{v}_g}{dt} = \frac{\partial \mathbf{v}_g}{\partial t} + V\,\frac{\partial \mathbf{v}_g}{\partial s} + w\,\frac{\partial \mathbf{v}_g}{\partial z} \qquad (2.50)$$

the total time-related change of $\mathbf{v}_g$ can be split up into the timely change at the fixed point, the change in the field along the horizontal streamline as well as the change in the vertical plane in the case of vertical motion of the particle.

If time-related density changes are neglected for the local change of $\mathbf{v}_g$, the following applies

$$\frac{\partial \mathbf{v}_g}{\partial t} = -\frac{1}{\varrho f}\,\nabla\left(\frac{\partial p}{\partial t}\right) \times \mathbf{k} \qquad (2.51)$$

so that in accordance with (2.49)

$$\mathbf{v}^* = -\frac{1}{\varrho f^2}\,\nabla\left(\frac{\partial p}{\partial t}\right) \qquad (2.52)$$

follows for the ageostrophic wind component associated with it. The vector of the local change thus runs parallel to the isallobars with the lower tendency values to the left while the ageostrophic component associated with local change perpendicularly intersects the isallobars and points from the pressure rise to the pressure fall (see Fig 2.17).

This ageostrophic wind component is called "isallobaric wind". It causes convergence of the air in the centre of the pressure fall and conversely divergence of the air in the centre of the pressure rise. If the surface field is considered, an ascending air motion above the area with pressure fall which can lead to cloud formation and precipitations as well as subsidence above the area with rise, which will be connected with cloud dispersion, occurs as a result of reasons of continuity.

Also in the arbitrarily selected situation of Fig 2.17, the aforementioned general rule can be verified. Because of the change field the geostrophic wind must turn to the left with time lapse and at the same time increase in strength. For this to happen the true winds must be both sub-geostrophic (on account of the change in direction) and also possess a component in regard to the low pressure (on account of the increase in speed).

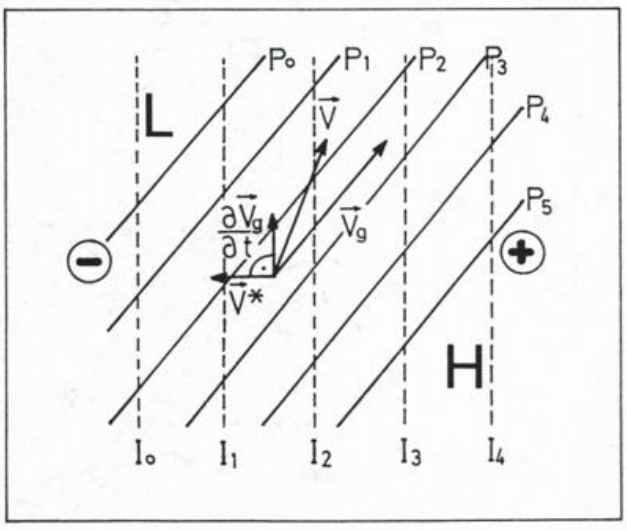

Fig. 2.17
Isallobaric wind (I_o, I_1 ... isallobars)

Regarding the discussion concerning the ageostrophic wind parts which occur in connection with changes of the geostrophic wind in the horizontal plane, the particle speed V should be replaced by V_g and the streamlines equated with the isobars for the sake of simplicity. In this case changes result and to be precise at the velocity where the isobars run together or apart (confluence or diffluence zone), as well as changes in direction along curved isobars.

These two possibilities can be represented mathematically if the natural coordinate system is used and the coordinate lies in the direction of the isobars. With a consideration as in 1.2

$$V_g \frac{\partial \mathbf{v}_g}{\partial s} = V_g \frac{\partial}{\partial s}(V_g \mathbf{t}) = V_g \frac{\partial V_g}{\partial s} t + \frac{V_g^2}{R_i} \mathbf{n}$$

or (2.53)

$$V_g \frac{\partial \mathbf{v}_g}{\partial s} = V_g \frac{\partial V_g}{\partial s} \mathbf{t} + V_g^2 K_i \mathbf{n}$$

is obtained.

R_i and K_i are the curved radius or curvature of the isobars here, positive in the case of cyclonic, negative in the case of anticyclonic curvature.

The first right-hand expression describes changes in speed, the second changes in direction of the geostrophic wind along the isobars. For the ageostrophic components linked with this, the following is true

$$\mathbf{v}^* = \frac{V_g}{f} \frac{\partial V_g}{\partial s} \mathbf{n} - \frac{V_g^2}{f} K_i \mathbf{t}. \qquad (2.54)$$

Fig 2.18 shows the relations in the area of a confluence and a diffluence zone through which particles flow. In the confluence zone the particles must increase their velocity for which ageostrophic motion to the lower pressure is required, in the diffluence zone they must reduce this, which is controlled by motion to the higher pressure.

These kinds of ageostrophic wind components are especially strong in the upper troposphere in the area of the jet streams. In the "entrance" and "exit" regions of a jet stream maximum, differences in the wind direction from the isohypse course between 20 and 30° often occur as a result.

In Fig 2.19 the relations in the area of curved isobars are shown whereby a constant speed V_g has been assumed for the sake of simplicity. It is seen that super-geostrophic

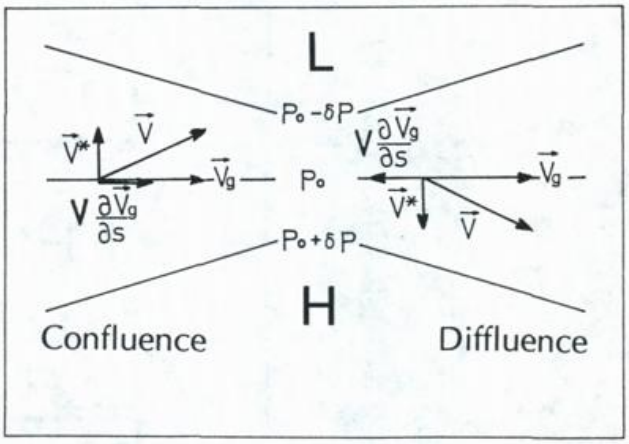

Fig. 2.18
Ageostrophic wind components with confluence and diffluence

winds result along anticyclonically curved isobars and subgeostrophic winds along cyclonically curved isobars. These differences in speed are a pre-requisite for a change in direction of the particles and correspond exactly to the gradient wind equilibrium described in 2.3. These are especially great in the waves of the upper current and particularly important in regard to the development of low pressure and high pressure systems.

Change of the wind and ageostrophic component with simultaneous vertical motion are correlated with the particular temperature field as $\partial \mathbf{v}_g/\partial z$ only depends on the isobaric temperature gradient in accordance with (2.35). The change vector lies parallel to the isotherms so that corresponding to

$$\mathbf{v}^* = -\frac{w}{f^2} \frac{g}{T} \nabla_p T \qquad (2.55)$$

the ageostrophic component lies across them and in the case of rising (w>0) is always directed from the warm to the cold side and in the case of descent (w<0) always from the cold to the warm side of the current (see Fig 2.20). While in the case of vertically uniform direction of the geostrophic wind, lateral deviations result, super-geostrophic winds occur in the case of warm air advection with rising as well as cold air advection with subsiding and conversely in the case of warm air advection with descent as

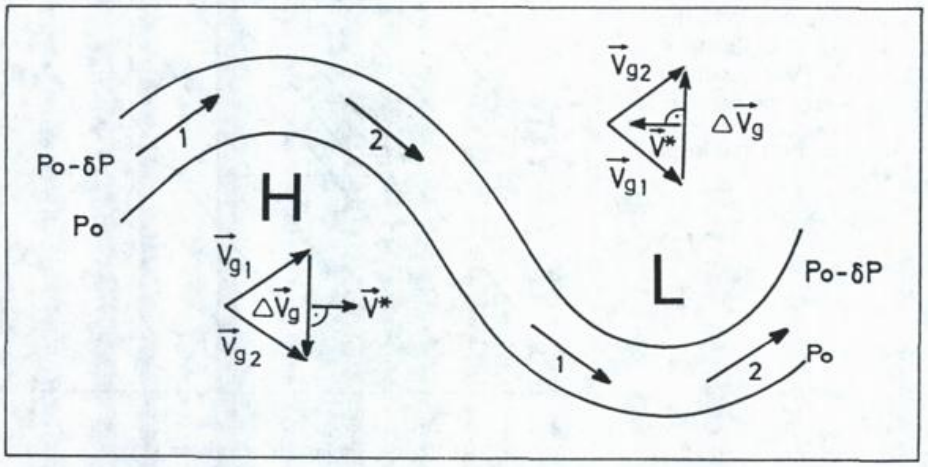

Fig. 2.19
Ageostrophic wind components inside curved isobars

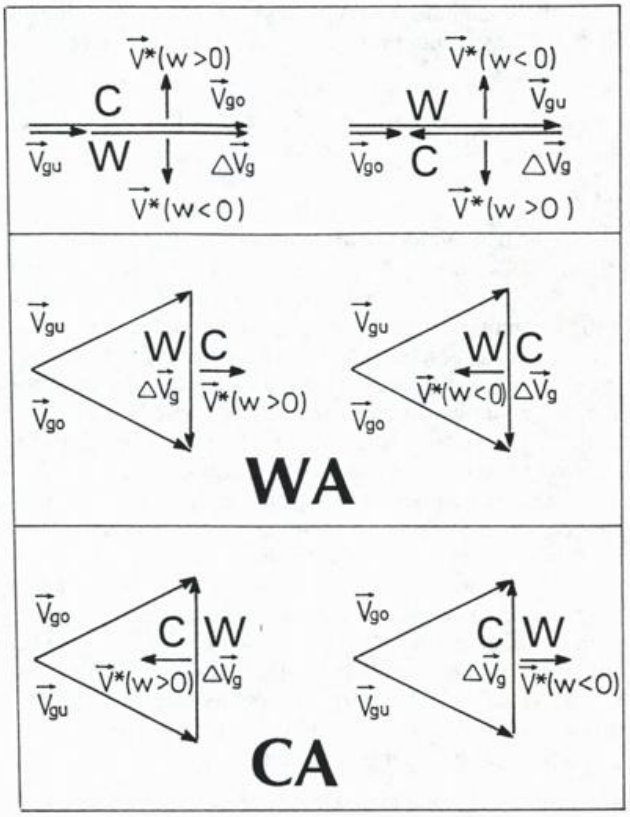

Fig. 2.20
Ageostrophic wind components in the case of vertical motion (V_{gu}, V_{go} geostrophic wind at the lower and upper level, resp.)

well as cold air advection with ascent, sub-geostrophic winds occur. These changes in direction and speed are necessary so that the rising or descending particle can match the geostrophic equilibrium of its new environment.

In a statistical investigation into ageostrophic wind components in the free atmosphere, KIEFER and FISCHER [7] referred especially to the importance of the last acceleration term. In their evaluation which was based on wind measurements over the British Isles, they found the remarkable fact that the difference in direction of the geostrophic wind is not independent of wind direction. Above 800 hPa southerly winds were correlated with an ageostrophic component towards the low geopotential and northerly winds with a component towards the high potential. A comparison with the three acceleration terms showed in this case that these differences in direction can be chiefly traced back to the effect of vertical motions. In the case of southerly winds it is on the front side of the tropospheric troughs where normally rising air motion is found (see 12.3). The ageostrophic component must then be directed there from the warm to the cold side of the current. As the troughs represent cold systems and isotherms and isohypses are mostly only at narrow angles to each other, this means at the same time that the ageostrophic component points to the low geopotential. The horizontal acceleration resulting from this is necessary so that the particle which has risen from a lower level of geostrophic speed can match the higher equilibrium speed of its new environment.

In the area of northerly winds on the rear side of the trough, the opposite effects result in the case of subsiding motion. A diagrammatic illustration of these phenomena is given in Fig 2.21.

2.11 Dynamic stability

More exact mathematical consideration shows that the ageostrophic wind components just described are not only correlated with the particular effective acceleration in regard to their amounts but also that the conditions in the stream field itself are important in this respect. It results that in the case of otherwise equal conditions the ageostrophic wind part in the area of cyclonic shear and/or curvature is especially small, in the area of anticyclonic shear and/or curvature on the other hand it is especially large.

The reason for this is the differing dynamic stability of the current. Stability in the case of horizontal or quasi horizontal disturbance motions of the particles is called dynamic stability. If such disturbance motion is slowed down, the current is dynamically stable, if it is increased the current is dynamically unstable.

A simple consideration will show how far shear influences the stability conditions. Assuming adiabatic conditions, a disturbance of the motion is studied on an isentropic sur-

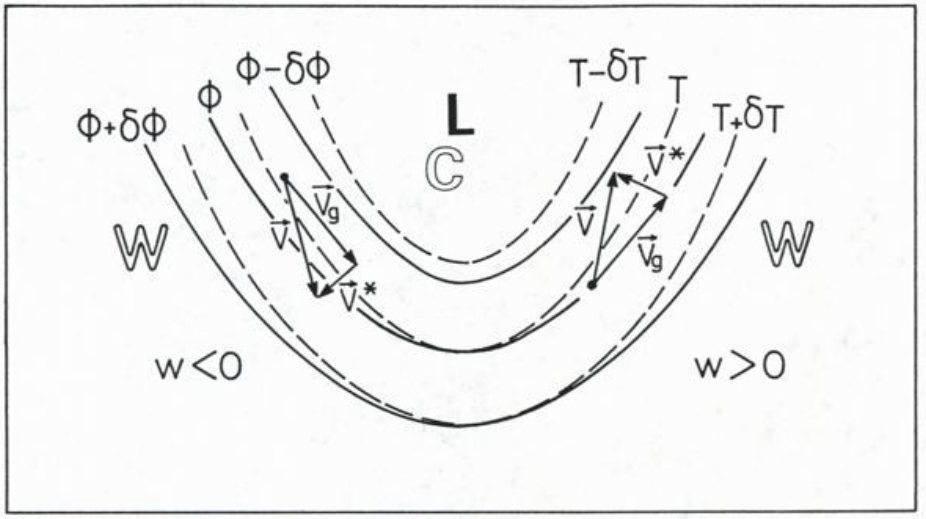

Fig. 2.21
Ageostrophic wind components in the vicinity of an upper trough (500 hPa). According to KIEFER and FISCHER [7]

face. The stream field is stationary in respect to time, in geostrophic equilibrium and has no change in the direction of the flow. A lateral change in velocity i.e. shear, is permitted.

We again use a natural coordinate system with the s-coordinate in the direction of the current. The motion component of the particle in this direction is V. At the beginning, let us say:

$$V = V_g.$$

Then the particle is subjected suddenly to a disturbance motion, with the speed V_N^* across the current. In this case

$$\frac{dV}{dt} = f V_N^*; \quad \frac{dV_N^*}{dt} = -f(V - V_g)$$

applies for the individual changes of V and V_N^*. In addition the particle experiences a change in the geostrophic wind during its lateral motion in accordance with

$$\frac{dV_g}{dt} = V_N^* \frac{dV_g}{\partial n}.$$

If now

$$\frac{dV}{dt} > \frac{dV_g}{dt},$$

$V > V_g$ is also the case after some time due to which with $dV_N^*/dt < 0$ damping of the disturbance results. The configuration is dynamically stable and the particle will turn round sooner or later and find its equilibrium again through oscillations. On the other hand if $dV/dt < dV_g/dt$, $V < V_g$ also is the case and with $dV_N^*/dt > 0$ the disturbance motion is further increased. The configuration is dynamically unstable so that the particle moves further away from its original position with increasing velocity.

From the equations for dV/dt and dV_g/dt, the conditions for dynamic stability or instability result immediately.

$$\left(f - \frac{\partial V_g}{\partial n}\right)_\theta \begin{matrix} > \\ = 0 \\ < \end{matrix} \begin{matrix} \text{Stable} \\ \text{Dynamically indifferent} \\ \text{Unstable} \end{matrix} \qquad (2.56)$$

is obtained.

It is seen that stream fields without shear are stable and stream fields with cyclonic shear of the geostrophic wind $(\partial V_g/\partial n < 0)$ are especially stable with these kinds of disturbance motions, i.e. also with additional ageostrophic components as described above. In the area of anticyclonic shear $(\partial V_g/\partial n > 0)$, stability on the other hand is minimal and if the amount of shear reaches or exceeds that of the Coriolis parameter, change to indifference or even to instability occurs. Observations show that dynamic instability occurs only on rare occasions at the mostly flat inclined surfaces of potential temperature and cannot continue for a long time before at least indifference is reached, as a result of changes in the wind field. In spite of that, the threshold to instability is not seldom passed over during the ascending motion of saturated air along the distinctly steeper oriented surfaces of pseudo-potential temperature. This leads to strongly accelerated vertical motions and to the formation of band-like zones with heavy precipitation („symmetric instability", comp. 5.6.4 and 7.3.3)

The difference in the dynamic stability of currents in which the particles pass through curved trajectories results from the relations for gradient wind equilibrium. In the area of cyclonic trajectories stability prevails; in the area of anticyclonic trajectories a change to instability occurs if, in the case of a given curved radius, the wind speed exceeds a critical value which can be read from (2.10).

3 Principles of dynamics

In this section firstly four parameters are introduced by which the horizontal stream field can be described with fair approximation. The equations in which these parameters appear represent the theoretical basis of modern synoptic meteorology.

3.1 Characteristics of the horizontal stream field

The horizontal wind vector is determined in a normal Cartesian coordinate system with the components u and v. The distribution of u and v can be described by a Taylor expansion.

$$\left.\begin{aligned} u &= u_0 + \left(\frac{\partial u}{\partial x}\right)_0 x + \left(\frac{\partial u}{\partial y}\right)_0 y + \cdots \\ v &= v_0 + \left(\frac{\partial v}{\partial x}\right)_0 x + \left(\frac{\partial v}{\partial y}\right)_0 y + \cdots \end{aligned}\right\} \begin{array}{l}\text{Derivations}\\ \text{of higher}\\ \text{order}\end{array} \qquad (3.1)$$

The subscript 0 in this case identifies the values or derivations at the coordinate origin. The higher the derivations used, the more exact the wind field will be represented.

With limitation to the first derivation, an initial linear approximation for the description of the stream field is obtained. If sums and differences of the derivation are obtained, the following is true for it:

$$\begin{aligned} u &= u_0 - \frac{1}{2}\left(\frac{\partial v}{\partial x} - \frac{\partial u}{\partial y}\right)_0 y + \frac{1}{2}\left(\frac{\partial u}{\partial x} + \frac{\partial v}{\partial y}\right)_0 x \\ &\quad + \frac{1}{2}\left(\frac{\partial u}{\partial x} - \frac{\partial v}{\partial y}\right)_0 x + \frac{1}{2}\left(\frac{\partial v}{\partial x} + \frac{\partial u}{\partial y}\right)_0 y \\ v &= v_0 + \frac{1}{2}\left(\frac{\partial v}{\partial x} - \frac{\partial u}{\partial y}\right)_0 x + \frac{1}{2}\left(\frac{\partial u}{\partial x} + \frac{\partial v}{\partial y}\right)_0 y \\ &\quad - \frac{1}{2}\left(\frac{\partial u}{\partial x} - \frac{\partial v}{\partial y}\right)_0 y + \frac{1}{2}\left(\frac{\partial v}{\partial x} + \frac{\partial u}{\partial y}\right)_0 x. \end{aligned} \qquad (3.2)$$

Four parameters which alone or in any desired combination characterise the linear stream field are defined by the values at the coordinate origin and the terms in brackets. These are

u_0, v_0	translation
$\left(\frac{\partial u}{\partial x} - \frac{\partial v}{\partial y}\right); \left(\frac{\partial v}{\partial x} + \frac{\partial u}{\partial y}\right)$	deformation
$\left(\frac{\partial u}{\partial x} + \frac{\partial v}{\partial y}\right)$	divergence
$\left(\frac{\partial v}{\partial x} - \frac{\partial u}{\partial y}\right)$	rotation (vorticity)

3.1.1 Translation

The following applies for the streamlines of pure translation

$$\frac{\partial y}{\partial x} = \frac{v}{u} = \frac{v_0}{u_0}.$$

Integration leads to (3.3)

$$y = \frac{v_0}{u_0} x + k \qquad (k \text{ integration constant})$$

This equation describes a pattern of straight streamlines of equal inclination and equal distance apart (Fig 3.1). They are identical in the equilibrium with the pressure field to isobars or isohypses.

An air parcel drifts in a time-related stationary translation field with uniform speed in a straight line without changing its form or outline. As a typical example of a translatorial component of the current we mention the western basic flow of the mid latitudes.

3.1.2 Deformation

In stream fields with deformation, the particles experience a change in their form. This can occur on the one hand through stretching or shrinking or on the other by shear.

Stretching deformation is defined by

$$\frac{\partial u}{\partial x} - \frac{\partial v}{\partial y}.$$

$$\frac{\partial y}{\partial x} = -\frac{y}{x} \qquad (3.4)$$

is obtained for the streamline and integrated

$$x\,y = k.$$

This equation describes hyperbolic streamlines which asymptotically approach the x and y axes (Fig 3.2). Also here equilibrium with the pressure field is conceivable. The deformation field is in this case identical to a four centre pressure pattern, with a col in the centre.

A particle which is located in a similar, time-related stationary field changes its form by being stretched along the x-axis and by being compressed along the y-axis. Therefore the x-axis is called the stretching axis or dilatation axis and the y-axis the shrinking axis. If only deformation is effective, its horizontal cross section remains constant despite the change in form of the particle.

In the case of shear deformation which is defined by

$$\frac{\partial v}{\partial x} + \frac{\partial u}{\partial y} \qquad (3.5)$$

horizontal shear of the wind causes the change in form of the particles (see Fig 3.3). However, rotation of the coordinate system by 45° is sufficient to change the shear field into the stretching field. It is therefore in principle not necessary to distinguish between both types of deformation.

In regard to the order of magnitude the deformation can be approximated by

$$\frac{\partial u}{\partial x} - \frac{\partial v}{\partial y} \sim \frac{U}{L} \qquad (3.6)$$

With a characteristic speed of 10 ms^{-1} and horizontal scale of $L = 10^6$m a dimension of $10^{-5}s^{-1}$ results in the Large Scale. However, $10^{-4}s^{-1}$ can also be reached in some areas.

Deformation is especially important for the origin of large horizontal temperature gradients arising in the area of thermal frontal zones (frontogenesis, see 7.2).

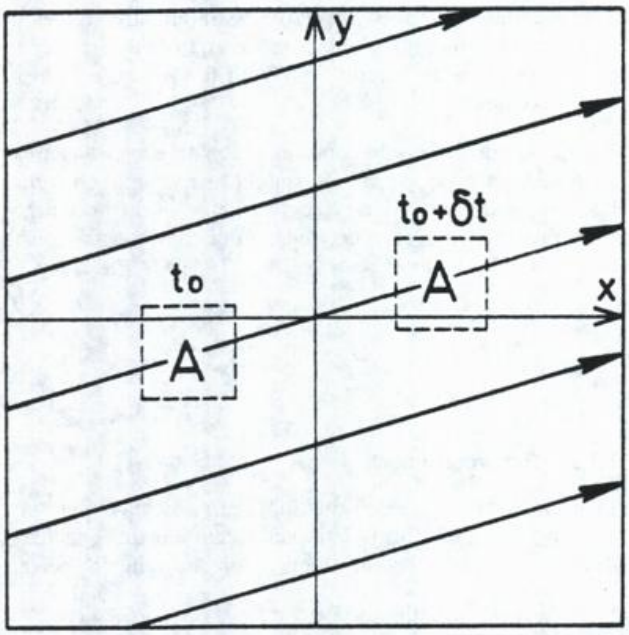

Fig. 3.1
Streamlines of pure translation
(broken outline of an air mass with horizontal cross section A)

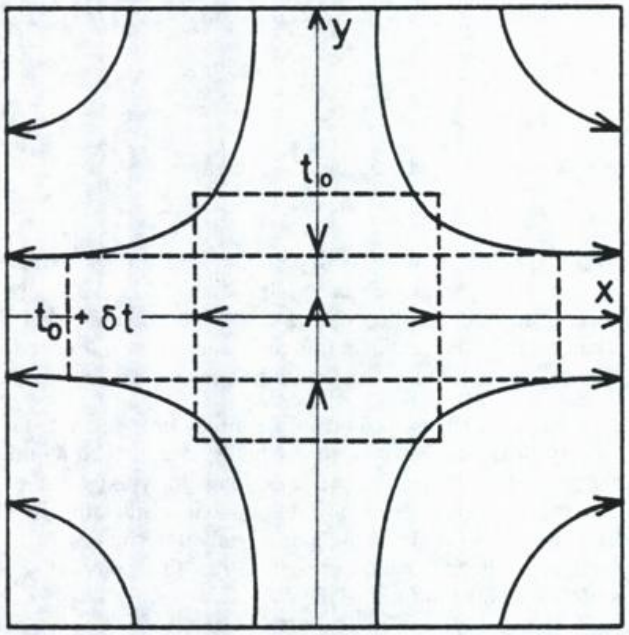

Fig. 3.2
Streamlines of pure stretching deformation

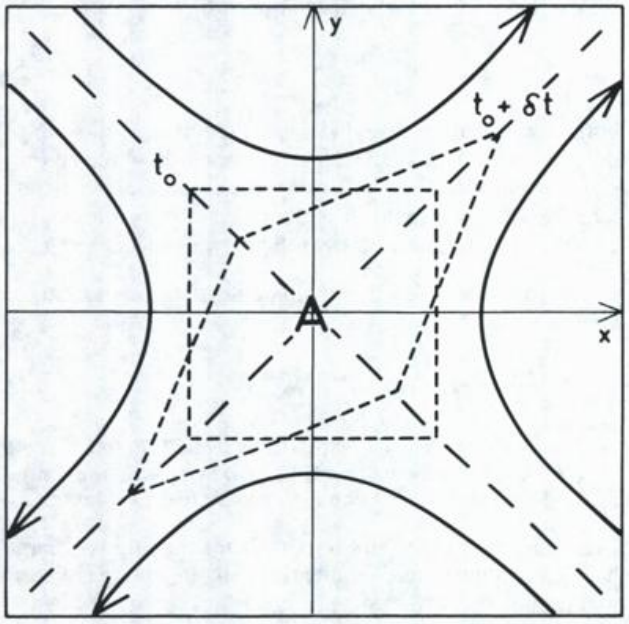

Fig. 3.3
Streamlines of pure shear deformation

Fig 3.4 shows fields in which deformation has been combined with translation. In the case of translation in the direction of the stretching axis, the image of a confluence zone results, in the case of translation in the direction of the shrinking axis, the image of a diffluence zone results. The changes in form in these fields occur with simultaneous transport of the air.

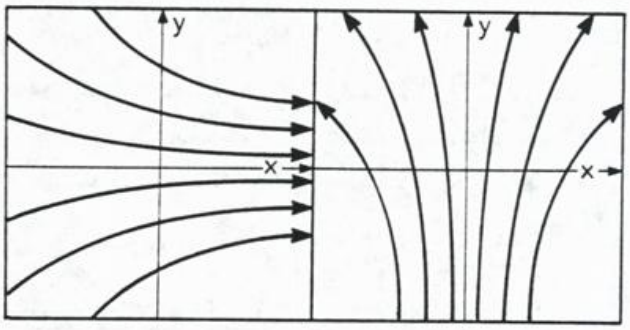

Fig. 3.4
Combination of deformation and translation

3.1.3 Divergence

Divergence of the horizontal stream field is described by

$$\nabla \cdot \mathbf{v} = \frac{\partial u}{\partial x} + \frac{\partial v}{\partial y}. \tag{3.7}$$

$$\frac{\partial y}{\partial x} = \frac{y}{x}; \quad y = k\,x$$

applies to the streamlines of pure divergence.

These are straight lines which emerge in the case of positive divergence at the coordinate origin and diverge on all sides while those in the case of negative divergence (convergence) move together at the origin (Fig 3.5). They therefore describe, in the case of divergence, streaming about a point- shaped source, in the case of convergence, streaming about a point-shaped sink of the stream field. The speed of the motion increases in this case outwards.

An air parcel, which is subject to divergence, stretches out horizontally and expands its cross section. In the case of convergence, however, it shrinks and its cross section becomes smaller. With the area A of the cross section, the divergence can alternatively be defined by

$$\nabla \cdot \mathbf{v} = \frac{1}{A}\frac{dA}{dt} \tag{3.8}$$

In Fig 3.5 it can be seen immediately that no equilibrium with the pressure field is conceivable for the streamlines of pure divergence. The divergence will therefore only appear as an additional component to the balanced part of the flow.

In the natural coordinate system the expression

$$\nabla \cdot \mathbf{v} = \frac{\partial V}{\partial s} + V\frac{\partial \beta}{\partial n}, \tag{3.9}$$

is obtained for horizontal divergence, whereby β represents the wind direction. The divergence accordingly consists of two components – velocity divergence $\partial V/\partial s$ and direction divergence $V\,\partial\beta/\partial n$. If the velocity along the streamlines increases (decreases), velocity divergence (convergence) results. If the streamlines converge (diverge) in the direction of the wind, direction convergence (divergence) is dominant (Fig 3.6).

In a field of pure divergence as shown in Fig 3.5 the particles are subject to both direction as well as velocity divergence. In reality, however, this can only occur infrequently or only for a short time. It can easily be seen that both parts of divergence will more likely have contrary signs and compensation must therefore be attempted. On account of the tendency to equilibrium, wind speed and streamline distance are namely generally conversely proportional. In a confluence zone of the flow e.g. (see Fig 3.7) direction convergence combined with velocity divergence is therefore found, in a diffluence zone conversely, direction divergence combined with velocity convergence. Which part is greater in individual cases and determines the sign of horizontal divergence cannot be decided immediately. It is therefore basically wrong to attempt to conclude only from

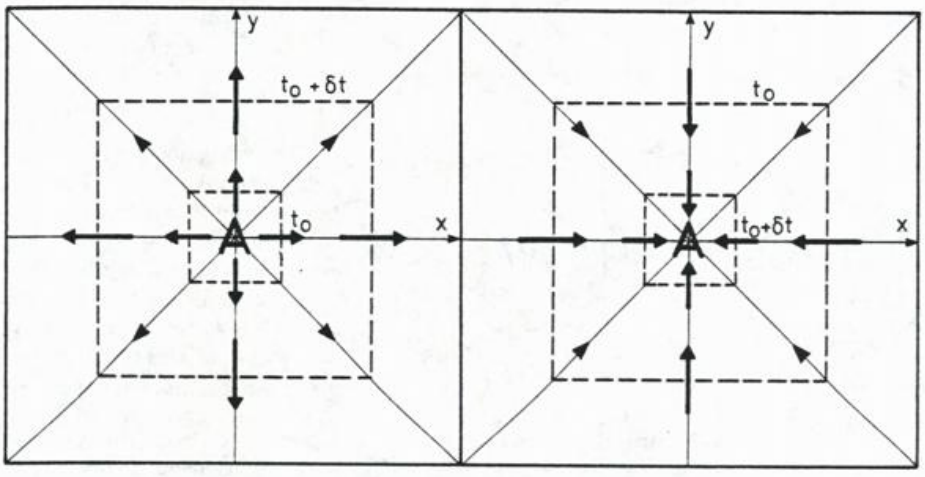

Fig. 3.5
Streamlines of pure horizontal divergence (left) and convergence (right)

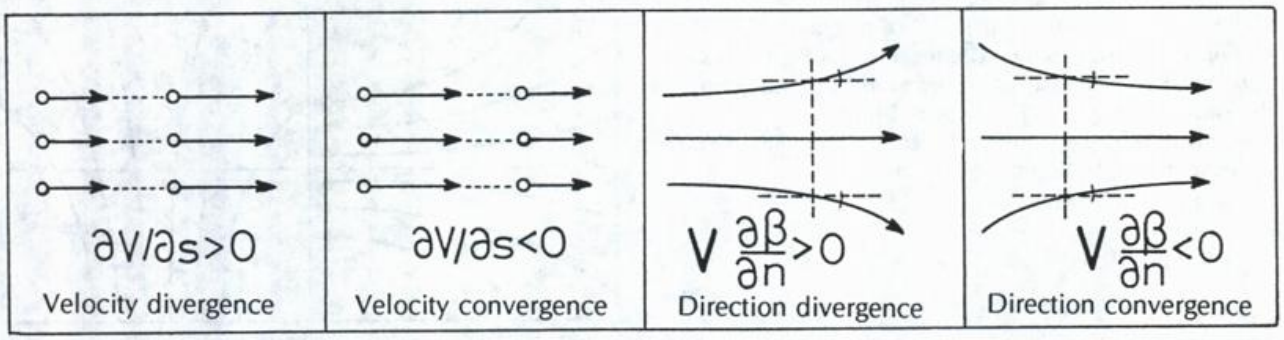

Fig. 3.6
Velocity and direction divergence

the diverging or converging of isobars or isohypses horizontal divergence or convergence.

On account of this tendency to compensate, the dimension of the horizontal divergence is generally very small. Although the two components have each an order of magnitude of $10^{-5}s^{-1}$ according to

$$\frac{\partial u}{\partial x}+\frac{\partial v}{\partial y}\sim\frac{U}{L} \tag{3.10}$$

the sum is one power of ten less, due to the mostly opposite signs and has the dimension $10^{-6}s^{-1}$ in the Large Scale. Only during synoptic developments, especially during the cyclogenesis, does the order of magnitude increase up to the value of $10^{-5}s^{-1}$ in the area concerned.

In order to get an idea of these dimensions, a time-related constant divergence or convergence is assumed. Then (3.8) can be integrated to

$$A = A_0\, e^{(\overline{\nabla\cdot v})t} \tag{3.11}$$

The content of the cross section of a particle in this case changes according to an e-function, whereby it lasts 10^5-10^6s ≈ 1–10 days until the area has stretched out, times the e-factor through divergence, or has shrunk to the e-th part through convergence. In the case of convective developments in the small or meso scale in which divergence can be $10^{-3}s^{-1}$, the same cross section changes occur, however, in less than half an hour!

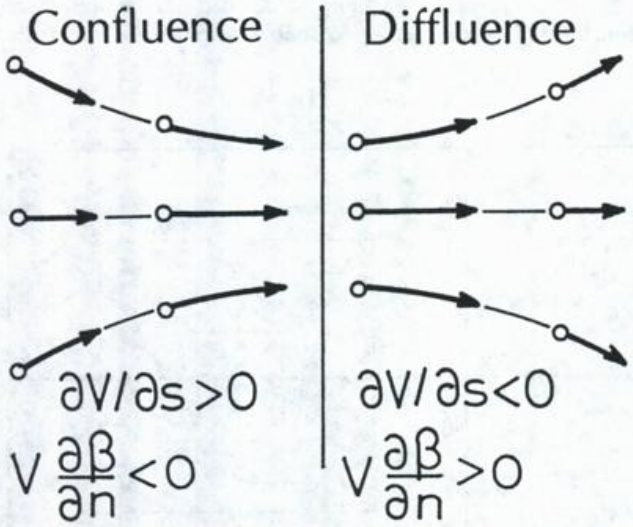

Fig. 3.7
Velocity and direction divergence in the area of confluence and diffluence zones

According to the reasoning given above, it is clear that the horizontal divergence is determined by the ageostrophic wind components considered in 2.10. However, also the geostrophic wind itself contains a divergent part. Based on the definitions in (2.6) and (2.30)

$$\nabla\cdot\mathbf{v}_g = -\frac{v_g}{f}\beta-\frac{1}{\varrho}\mathbf{v}_g\cdot\nabla\varrho \tag{3.12}$$

is obtained in the z-system and

$$\nabla_p\cdot\mathbf{v}_g = -\frac{v_g}{f}\beta$$

in the p-system

whereby $\beta\equiv\frac{\partial f}{\partial y}$ is described as ROSSBY parameter. It has the magnitude of $10^{-11}s^{-1}m^{-1}$.

In both equations a term with the meridional component of the geostrophic wind appears. Divergence results with $v_g<0$ for motion to the south, convergence with $v_g>0$ for motion to the north. These divergences result due to the spherical form of the earth and correspond to the direction divergence or convergence of the meridians. Its magnitude is $10^{-6}s^{-1}$ and corresponds to the generally valid dimension of the divergence in the Large Scale.

In the equation in the z-system an additional term appears with density advection. Divergence results in the case of advection of denser, convergence in the case of advection of less dense air. This results from the fact that in otherwise equal conditions, the geostrophic wind in air of greater density is weaker than in air of less density.

On account of the small dimension of the divergence, it is problematic to try to calculate the divergence directly from wind measurements. Although the method for this is very simple – only fields of both wind components or their values at certain grid points are needed -, the results would be extremely prone to error on account of the inaccuracy of wind measurements and should only be used with caution. As on the other hand knowledge of divergence represents an essential requirement for understanding synoptic processes, indirect methods of determination must be used. A good possibility for this is provided by the equation of vorticity which is discussed in Section 3.4.

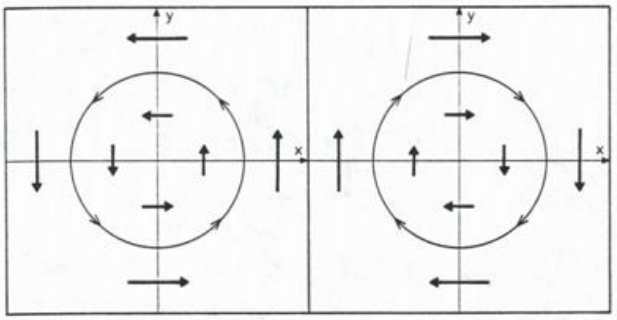

Fig. 3.8
Streamlines of pure rotation (left cyclonic, right anticyclonic)

3.1.4 Rotation (vorticity)

The fourth characteristic parameter describes rotational motion components in the horizontal stream field. A distinction between relative and absolute rotation or vorticity is made. Relative vorticity reflects the rotation around a vertical axis relative to the earth and is defined by the vertical component of the rotor of the three dimensional wind vector

$$\zeta \equiv \mathbf{k} \cdot (\nabla_3 \times \mathbf{v}_3) = \frac{\partial v}{\partial x} - \frac{\partial u}{\partial y}. \tag{3.13}$$

In the case of absolute vorticity η which is related to an absolute fixed star oriented system, the particular component of the earth's rotation is also included which is exactly $f = 2\,\Omega \sin\varphi$:

$$\eta = \zeta + f = \frac{\partial v}{\partial x} - \frac{\partial u}{\partial y} + f. \tag{3.14}$$

$$\frac{\partial y}{\partial x} = -\frac{x}{y}, \tag{3.15}$$

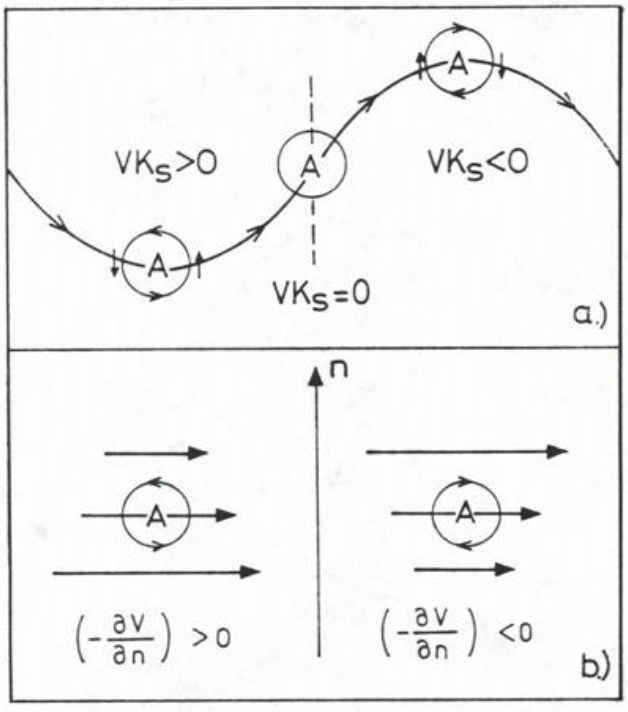

Fig. 3.9
Curvature and shear vorticity

applies for the streamlines of pure rotation which when integrated produces

$$x^2 + y^2 = k$$

These streamlines are therefore concentric circles around the coordinate origin, whereby velocity increases outwards. Circles in the anti-clockwise direction have positive, circles in the clockwise direction negative relative vorticity (Fig 3.8).

In contrast to divergence, but similar as in the case of translation and deformation, equilibrium with the pressure field is possible for a field of pure vorticity. The circles of Fig 3.8 can therefore also be understood as isobars or isohypses and then describe a low in the area of positive or a high in the area of negative rotation. On account of this connection the words cyclonic or anticyclonic vorticity are also frequently used for rotation of positive or negative signs.

In the natural coordinate system we obtain

$$\zeta = VK_s - \frac{\partial V}{\partial n} \tag{3.16}$$

with the streamline curvature K_s positively numbered in the case of cyclonic, negatively numbered in the case of anticyclonic curvature. Similar to divergence, vorticity also consists therefore of two components – curvature vorticity VK_s and shear vorticity $(-\partial V/\partial n)$. In the area of cyclonically (anticyclonically) curved streamlines, the particles have positive (negative) curvature vorticity, whereby the amount increases proportionally to wind speed. If the speed decreases (increases) to the left when looking in the wind direction, the particles have positive (negative) shear vorticity (Fig 3.9).

The magnitude of absolute vorticity is determined by f and is $10^{-4}s^{-1}$. The magnitude of relative vorticity lies approximately in accordance with the scale-approximation at $10^{-5}\ s^{-1}$ but can increase in individual areas or at certain levels up to $10^{-4}s^{-1}$. If, for example, the curvature radius of the streamlines is assumed as $K_s = \pm 500$ km, the curvature vorticity at $V = 10\ ms^{-1}$ is $VK_s = \pm 2 \times 10^{-5}s^{-1}$. This will be typical for the surface field and the lower troposphere. At the jet stream level, however, $V = 50\ ms^{-1}$ can be used in this calculation and $VK_s = \pm 1 \times 10^{-4}s^{-1}$ is obtained. Similarly to this $\pm 2 \times 10^{-5}s^{-1}$ results with a lateral speed drop of $10\ ms^{-1}$ over 500 km distance, however, in the case of 50 $ms^{-1} \pm 10^{-4}s^{-1}$ results. Such major shear, however, is not unusual at the fringes of the jet streams.

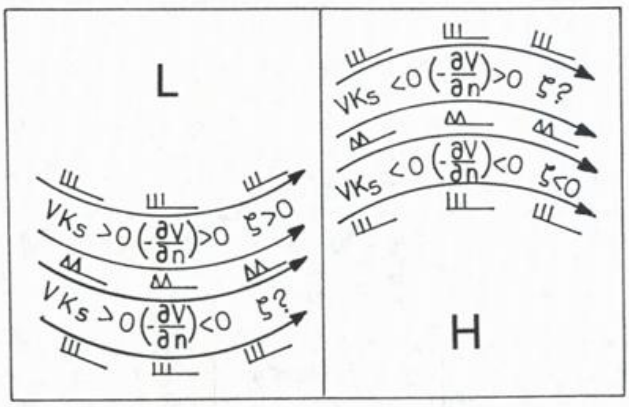

Fig. 3.10
Combination of curvature and shear vorticity

The two parts of relative vorticity can – similar to the case of divergence – compensate each other, but can also – in contrast to divergence – overlap and therefore reinforce each other. If a wind maximum is observed – looking in the direction of flow – cyclonic shear vorticity is found on its left fringe and on its right fringe anticyclonic shear vorticity. In the case of simultaneous cyclonic curvature of the streamlines, cyclonic curvature vorticity on the left fringe adds to this, while on the right fringe, compensation can be seen. Conversely, in the case of anticyclonic curvature, the cyclonic shear vorticity on the left side is weakened by the curvature effect, while on the right fringe shear and curvature term have an equally negative sign (Fig 3.10).

Nevertheless, the negative relative vorticity cannot be of any magnitude as otherwise the wind field would lose its dynamic equilibrium. Corresponding to the discussion in 2.11, the limit condition applying to this is that the absolute vorticity of the geostrophic wind determined on isentropic surfaces must be

$$\eta_{g\Theta} = (\zeta_g + f)_\Theta \geq 0$$
$$= \left(V_g K_i - \frac{\partial V_g}{\partial n} + f \right)_\Theta \geq 0 \qquad (3.17)$$

This means that the anticyclonic relative vorticity of the geostrophic wind must not exceed the value of f in total. With initial approximation this also applies for the vorticity of the true wind. In the above-quoted examples for curvature and shear vorticity in the jet stream where $1 \times 10^{-4} s^{-1}$ as amount resulted, the limit value would be just reached in the anticyclonic case in the middle latitudes, the flow therefore being in a dynamically indifferent state.

When using this equation in practice, the difference between the vorticity on Θ-surfaces and on p-surfaces must be considered in the case of baroclinity. If only shear vorticity is considered

$$\left(f - \frac{\partial V}{\partial n} \right)_p = \left(f - \frac{\partial V}{\partial n} \right)_\Theta + \frac{\partial V}{\partial z} \operatorname{tg} \alpha_i \qquad (3.18)$$

is true, whereby α_i describes the angle between pressure – and isentropic surfaces, normal to the wind direction. In sharply inclined baroclinic zones with major vertical wind change, anticyclonic shear and minor absolute vorticity can occur accordingly on Θ-surfaces together with cyclonic shear and corresponding major vorticity on the p-surfaces. Therefore no clear conclusion can be drawn in regard to the level of stability of the current from a calculation of vorticity only on the pressure surfaces. For saturated air the conditions on surfaces of pseudopotential temperature have to be considered.

Streamline patterns are shown in Fig 3.11 in which rotation combined with other characteristics of the flow occurs. In conjunction with a large translatory component, wave-shaped streamlines with troughs and ridges result, as characteristic of the middle and upper troposphere. If translation is relatively weak, closed streamlines are embedded into the waves, which correspond to low and high pressure areas. These kinds of fields are typical for the flow in the lower troposphere near to the surface.

If rotation and deformation overlap in equal amounts, the image of a shear zone results. In the case of heavier rotation, the streamlines take on an elliptic form. Spiral-shaped streamlines, however, result from a combination of rotation and divergence.

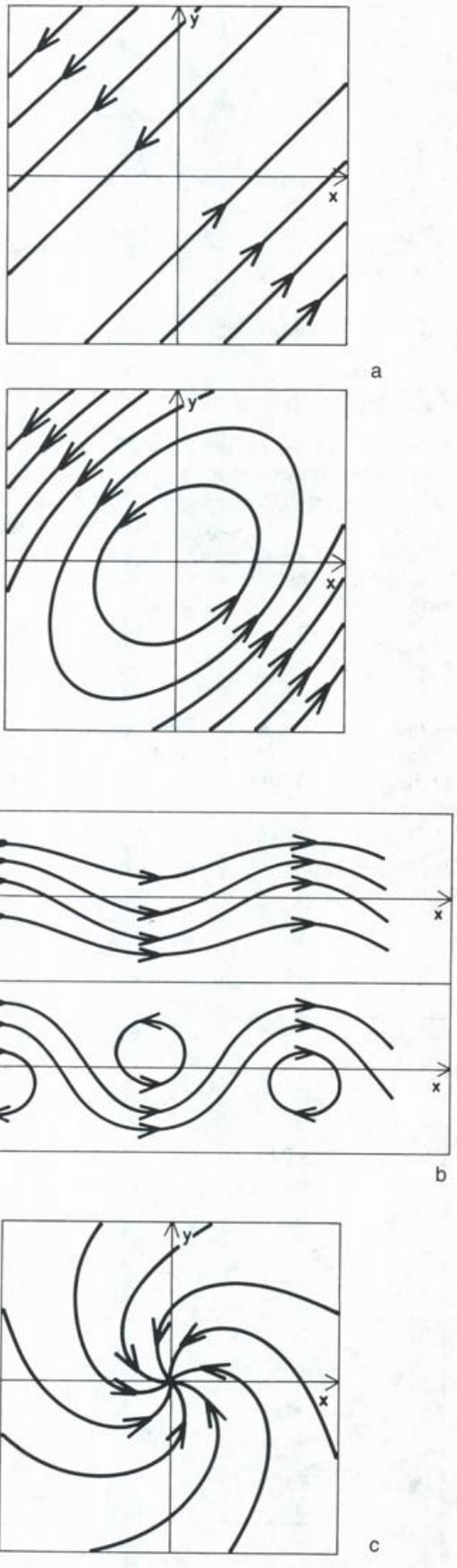

Fig. 3.11
(a) Combination of cyclonic rotation and deformation
(b) Combination of rotation and translation
(c) Combination of cyclonic rotation and horizontal convergence

3.1.5 Computation of vorticity

Knowledge of the vorticity field is a pre-requirement for many diagnostic applications. The definition of vorticity required for this is most easily obtained by means of geostrophic approximation. Here the true or measured wind is replaced by the geostrophic equilibrium wind and its rotatory component is calculated.

With

$$u_g = -\frac{1}{f}\frac{\partial \Phi}{\partial y}, \quad v_g = \frac{1}{f}\frac{\partial \Phi}{\partial x}$$

results for

$$\zeta_g = \frac{\partial v_g}{\partial x} - \frac{\partial u_g}{\partial y} = \frac{1}{f}\left(\frac{\partial^2 \Phi}{\partial x^2} + \frac{\partial^2 \Phi}{\partial y^2}\right) - \frac{1}{f^2}\frac{\partial \Phi}{\partial y}\frac{\partial f}{\partial y} = \frac{1}{f}\nabla^2 \Phi + \frac{u_g}{f}\beta. \tag{3.19}$$

As the second term on the right has a magnitude of $10^{-6}s^{-1}$, it can be neglected without further consideration and

$$\zeta_g = \frac{1}{f}\nabla^2 \Phi \tag{3.20}$$

and also

$$\eta_g = \frac{1}{f}\nabla^2 \Phi + f$$

are obtained with good approximation.

For practical calculations the differential quotients must be changed to difference quotients. A square grid, as shown in Fig 3.12 with four points which lie at equi-distance d from the centre point, is used for this purpose. With the aid of this it is immediately seen that the two derivations of Φ can be approximated for the centre point in the form of

$$\frac{\partial^2 \Phi}{\partial x^2} \approx \frac{\Phi_1 - 2\Phi_0 + \Phi_3}{d^2}, \quad \frac{\partial^2 \Phi}{\partial y^2} \approx \frac{\Phi_2 - 2\Phi_0 + \Phi_4}{d^2}$$

Therefore

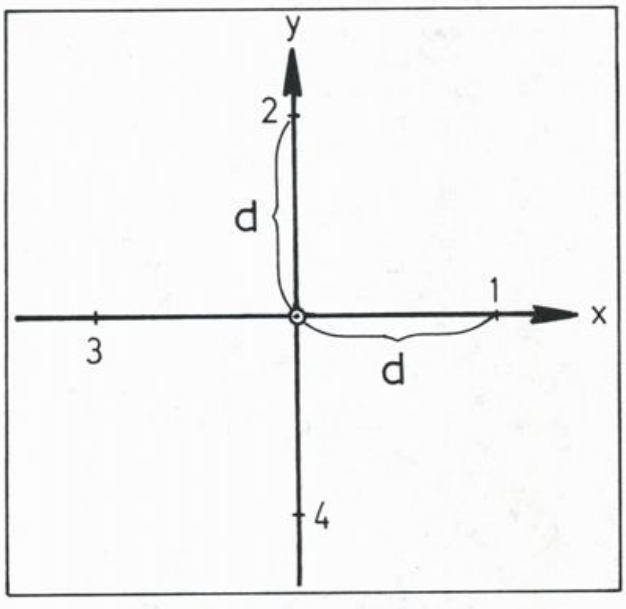

Fig. 3.12
Grid for calculating vorticity

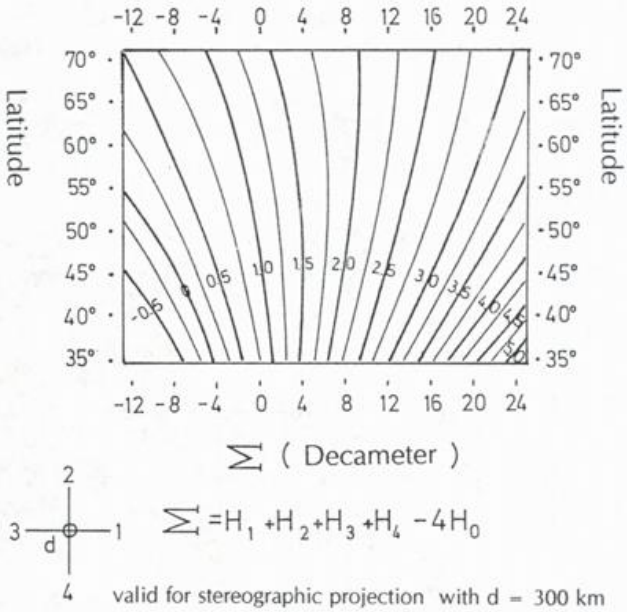

Fig. 3.13
Nomogramm for computation of absolute geostrophic vorticity (in 10^{-4} s^{-1})

results for the Laplace of Φ

$$\nabla^2 \Phi \approx \frac{\Phi_1 + \Phi_2 + \Phi_3 + \Phi_4 - 4\Phi_0}{d^2} \tag{3.22}$$

When doing the calculations, the distortion of the map projection (scale factor: m) and the definition of geopotential (2.3) must be taken into consideration, so that the formula for geostrophic absolute vorticity which can be used practically reads as follows:

$$\eta_g = \frac{g\,m^2}{fd^2}(H_1 + H_2 + H_3 + H_4 - 4H_0) + f. \tag{3.23}$$

H_n here means data of height of the topography concerned in [m] which are numerically identical with the geopotential data in [gpm]. The value 9.8 ms $^{-2}$ must be used accordingly for gravity acceleration g.

The nomogramme reproduced in Fig 3.13 can be used for calculating vorticity manually. It is valid for maps with stereographic projection and equates to a grid distance of d = 300 km. With a pre-printed grid overlay the required figures can be very quickly read off and the value of absolute vorticity can be seen immediately from the total in consideration of the particular latitude. Naturally this process requires a carefully analysed potential field of the particular topography.

In practice manual calculation of vorticity at certain predefined points is sufficient, e.g. along one or several isohypses. A field distribution of absolute vorticity can be obtained by graphical or numerical methods. Examples of numerically calculated vorticity fields are provided in later chapters in connection with sample weather situations.

3.2 The equation of continuity

Mass can be neither created nor eliminated. If the mass flow is considered through a volume element $\delta x\,\delta y\,\delta z$, the net flow, i.e. the difference between inflow and outflow of

mass through the sides, must be equal, therefore, to the time-related mass accumulation within the volume element.

In the x-axis (of a Cartesian coordinate system, see Fig 3.14) the mass import is given by

$$\varrho u\, \delta y\, \delta z,$$

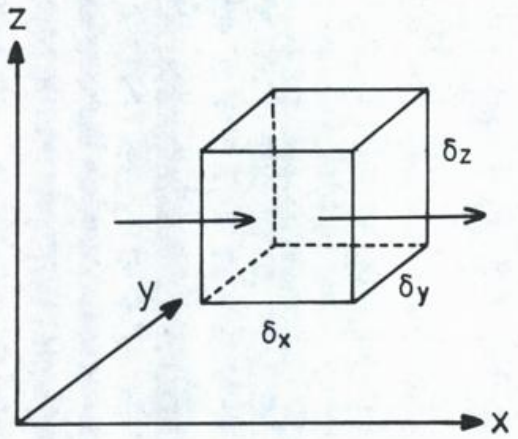

Fig. 3.14
For deriving the equation of continuity

the mass export by

$$\left[\varrho u + \frac{\partial}{\partial x}(\varrho u)\,\delta x\right] \delta y\, \delta z.$$

The difference between both expressions provides the net flow in the x-axis:

$$-\frac{\partial}{\partial x}(\varrho u)\,\delta x\, \delta y\, \delta z.$$

For the flows in the y and z axes, similar equations apply so that for total net flow into the volume element

$$-\left[\frac{\partial}{\partial x}(\varrho u) + \frac{\partial}{\partial y}(\varrho v) + \frac{\partial}{\partial z}(\varrho w)\right] \delta x\, \delta y\, \delta z$$

is obtained.

Divided by the volume $\delta x \delta y \delta z$ the net flow into the unit volume, which must be equal according to the above to the local time-related density change within the volume, is obtained. Therefore

$$\frac{\partial \varrho}{\partial t} = -\left[\frac{\partial}{\partial x}(\varrho u) + \frac{\partial}{\partial y}(\varrho v) + \frac{\partial}{\partial z}(\varrho w)\right]$$

is true or with the three-dimensional Nabla operator

$$\frac{\partial \varrho}{\partial t} = -\nabla_3 \cdot (\varrho\, \mathbf{v}_3). \tag{3.24}$$

This is the so-called equation of continuity. The expression $\nabla_3 \cdot (\varrho\, \mathbf{v}_3)$ represents the divergence of the three-dimensional mass flow and is described with a positive sign as mass divergence, with a negative sign as mass convergence. In the case of mass divergence – seen three-dimensionally – the density decreases locally, in the case of mass convergence it increases.

The expression $\nabla_3 \cdot (\varrho\, \mathbf{v}_3)$ can be split up so that

$$\frac{\partial \varrho}{\partial t} = -\mathbf{v}_3 \cdot \nabla_3 \varrho - \varrho\, \nabla_3 \cdot \mathbf{v}_3 \tag{3.25}$$

can also be written.

The first right-hand term is three-dimensional density advection. If denser (thinner) air is transported into the volume, the density in it must increase (decrease) locally.

$$\nabla_3 \cdot \mathbf{v}_3 = \frac{\partial u}{\partial x} + \frac{\partial v}{\partial y} + \frac{\partial w}{\partial z} \tag{3.26}$$

is three-dimensional wind divergence. It is composed of horizontal divergence $\nabla \cdot \mathbf{v} = \frac{\partial u}{\partial x} + \frac{\partial v}{\partial y}$ and vertical divergence $\frac{\partial w}{\partial z}$.

Horizontal divergence is a measure for the change in cross section, vertical divergence a measure for the change in vertical thickness of the air particles. Three-dimensional divergence describes the volume expansion or contraction which is caused by spatial differences of the wind accordingly.

In the case of divergence in the three-dimensional wind field the density must decrease locally, in the case of convergence it must increase.

For incompressible media in which density is invariant with changes of pressure, the equation of continuity takes on the form

$$\nabla_3 \cdot \mathbf{v}_3 = 0 \quad \text{or} \quad \nabla \cdot \mathbf{v} = -\frac{\partial w}{\partial z} \tag{3.27}$$

Horizontal divergence (convergence) is linked accordingly with vertical convergence (divergence) of equal magnitude so that three-dimensional divergence disappears. Although this equation cannot be applied directly to the air as gas mixture, observations in the large scale show a quasi-incompressible behaviour of the atmosphere.

This is clear if the equation of continuity is derived for the p-system and at the same time hydrostatic equilibrium is assumed. If a particle of the mass δM with sides δx, δy and δz which is located between pressure surfaces p and $p - \delta p$ is considered, δz can be replaced by δp in accordance with (2.2).

$$\delta z = \frac{\delta p}{g\, \varrho}$$

is true so that

$$\delta M = \frac{\delta x\, \delta y\, \delta p}{g}$$

is obtained for mass.

As mass remains constant with motion it follows

$$\frac{1}{\delta M}\frac{d}{dt}(\delta M) = \frac{g}{\delta x\, \delta y\, \delta p}\frac{d}{dt}\left(\frac{\delta x\, \delta y\, \delta p}{g}\right) = 0.$$

By conversion

$$\frac{1}{\delta x}\delta\left(\frac{dx}{dt}\right) + \frac{1}{\delta y}\delta\left(\frac{dy}{dt}\right) + \frac{1}{\delta p}\delta\left(\frac{dp}{dt}\right) = 0$$

is obtained from this and finally if exceeding the limit

$$\left(\frac{\partial u}{\partial x}+\frac{\partial v}{\partial y}\right)_p+\frac{\partial}{\partial p}\left(\frac{dp}{dt}\right)=0$$

or with $\omega \equiv dp/dt$ (3.28)

$$\nabla_p \cdot \mathbf{v}+\frac{\partial \omega}{\partial p}=0.$$

This is the equation of continuity for the p-system. Index p here means that horizontal divergence must not be determined on level surfaces but on pressure surfaces. The relation just obtained is clearer if transparency is created using the term with ω. It can be split up as total pressure change into

$$\omega \equiv \frac{dp}{dt}=\frac{\partial p}{\partial t}+\mathbf{v}\cdot\nabla p+w\frac{\partial p}{\partial z}. \quad (3.29)$$

The horizontal wind vector consists of a geostrophic part and a normally much smaller ageostrophic component

$$\mathbf{v}=\mathbf{v}_g+\mathbf{v}^*.$$

As, however, the product $\mathbf{v}_g \cdot \nabla p$ disappears

$$\omega=\frac{\partial p}{\partial t}+\mathbf{v}^*\cdot\nabla p-g\varrho w. \quad (3.30)$$

is true when using the hydrostatic equation.

The total time-related pressure change of a particle consists, therefore, of local pressure change at the fixed point, pressure change with ageostrophic motion across the isobars and pressure change with vertical motion. For synoptic systems the following magnitudes can be used for the three terms

$$\begin{aligned}&\frac{\partial p}{\partial t}\sim 10\ \text{h Pa/day}\\ &\mathbf{v}^*\cdot\nabla p\sim 1\ \text{ms}^{-1}\cdot 0.01\ \text{h Pa}\cdot\text{km}^{-1}\\ &\qquad\sim 1\ \text{h Pa/day}\\ &g\varrho w\sim 100\ \text{h Pa/day}\end{aligned} \quad (3.31)$$

The estimate for $g\varrho w$ is naturally only valid for free atmosphere as w must be zero on the ground. Therefore

$$\omega_0 \approx \frac{\partial p_0}{\partial t}$$

is true near the ground.

However, in free atmosphere

$$\omega \approx -g\varrho w \quad (3.32)$$

can be used with good approximation. ω describes in this case the vertical velocity in the the p-system, whereby, due to the sign change, negative values indicate an ascending motion, positive values a descending motion. Used in (3.28), the quasi-incompressible form of the equation of continuity results with

$$\nabla_p \cdot \mathbf{v}=-\frac{\partial w}{\partial z} \quad (3.33)$$

This means that horizontal divergence (convergence) must be linked on a pressure surface to vertical convergence (divergence) in equal amounts. If it is assumed that on average the maximum of the vertical motions will be found in the middle troposphere and that on the other hand at surface level and at greater heights (tropopause) vertical motions will disappear, then the distribution as shown diagramatically in Fig 3.15 will result

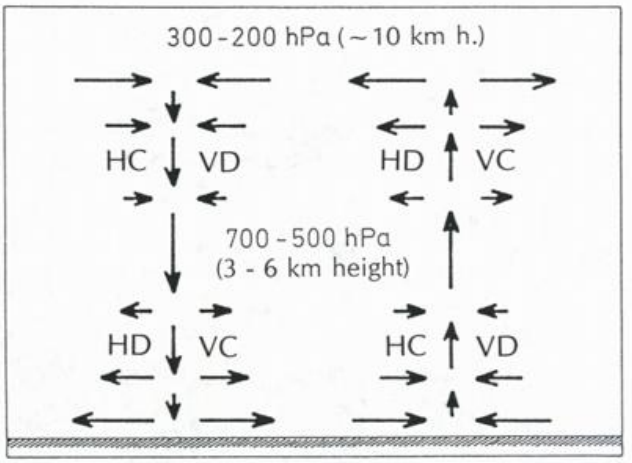

Fig. 3.15
Connection of horizontal and vertical divergence and convergence in the troposphere

3.3 The pressure tendency equation

With the aid of the continuity equation it is easy to derive the pressure tendency equation which provides insight into the physical background of pressure changes.

Assuming hydrostatic balance and integrating the hydrostatic equation (2.2), the following is true for pressure p at a defined level z

$$p=\int_z^\infty g\varrho\, dz. \quad (3.34)$$

From this the following results for local pressure tendency at this level

$$\left(\frac{\partial p}{\partial t}\right)_z=\int_z^\infty g\frac{\partial \varrho}{\partial t}dz \quad (3.35)$$

and using the continuity equation (3.24)

$$\begin{aligned}\left(\frac{\partial p}{\partial t}\right)_z&=-\int_z^\infty g\,\nabla_3\cdot(\varrho\mathbf{v}_3)\,dz\\ &=-\int_z^\infty g\,\nabla\cdot(\varrho\mathbf{v})\,dz-\int_z^\infty g\frac{\partial}{\partial z}(\varrho w)\,dz.\end{aligned} \quad (3.36)$$

Since w=0 when z=∞ the last term can be immediately integrated to $(g\varrho w)_z$. The local pressure tendency is therefore determined by the vertical integral of the horizontal mass divergence and by vertical motion. If the first right-hand term is again split up, the equation then reads

$$\begin{aligned}\left(\frac{\partial p}{\partial t}\right)_z&=-\int_z^\infty g\varrho\nabla\cdot\mathbf{v}\,dz\\ &-\int_z^\infty g\mathbf{v}\cdot\nabla\varrho\,dz+(g\varrho w)_z.\end{aligned} \quad (3.37)$$

The first right-hand term contains horizontal divergence of the wind field, the second density advection.

Corresponding to the equation, pressure increases at level z with

a) Horizontal convergence in the vertical integral above z ($\overline{\nabla \cdot \mathbf{v} < 0}$). As a result, mass is concentrated in the air column above z, so that its weight increases.
b) Cold air advection in the vertical integral above z ($\overline{-\mathbf{v} \cdot \nabla \varrho > 0}$). Less dense mass is replaced by more dense one so that the weight of the air column must increase.
c) Upwards motion at level z (w>0). As a result mass is pumped from below into the air column above z which also leads to an increase in weight.

Conversely, pressure decreases with

a) Horizontal divergence in the vertical integral above z
b) Warm air advection in the vertical integral above z and/or
c) Downwards motion at level z.

If the effect of vertical motions and horizontal vergences is compared, it becomes immediately clear that their contributions to pressure tendency will presumably always have opposite signs and therefore try to compensate. If, for example, pressure fall is triggered due to a downwards motion at level z, mass will flow in from the side, as a result of which the pressure fall will be reduced. The same can be expected if horizontal convergence is the first to take effect.

In regard to the order of magnitude of the contributions which the two types of horizontal mass convergence provide, it can be said that in general the effect of horizontal vergences in the wind field is greater by one to the power of ten than that of density advection. The reason for this is the fact that only advection with the ageostrophic wind part is able to provide a contribution to the change in pressure, while the normally dominant advection with the geostrophic wind is neutralised by divergence effect in the opposite direction (see 3.1.3).

If the relation (3.37) is applied to surface pressure tendency, distinction must be made between flat terrain where vertical motion vanishes and mountaineous terrain where vertical motions are forced. The following applies for flat terrain

$$\begin{aligned} \frac{\partial p_0}{\partial t} &= -\int_0^\infty g \nabla \cdot (\varrho \mathbf{v})\, dz \\ &= -\int_0^\infty g \varrho \nabla \cdot \mathbf{v}\, dz - \int_0^\infty g \mathbf{v} \cdot \nabla \varrho\, dz. \end{aligned} \tag{3.38}$$

Surface pressure tendency is therefore only determined by the integral over horizontal mass divergence in which, in accordance with the above argumentation, divergence of the wind field generally dominates. In the case of mountaineous terrain vertical divergence also comes into consideration and produces a contribution to pressure rise in the case of forced ascent, in the case of descent a contribution to pressure fall (see 14.3).

Occasionally pressure changes are differentiated dynamically and thermally and it is argued, for example, that pressure on the surface must fall if the air column above the place concerned is heated diabatically and therefore is reduced in density. This argument is not correct. Density changes by heating or cooling only lead to vertical expansion or shrinking of the air column and are therefore associated with pressure changes with height, but not, however, – as the total mass remains the same – to changes on the surface. Only if, as a consequence of vertical expansion by heating, the air begins to flow away with height divergently to the side, pressure starts to decrease on the surface as a consequence of the loss of mass, while with height the rise initially seen is reduced.

With the p-system the tendency equation takes on a more simple form. From the continuity equation (3.28)

$$\nabla_p \cdot \mathbf{v} = -\frac{\partial \omega}{\partial p} = -\frac{\partial}{\partial p}(dp/dt)$$

$$\frac{dp}{dt} = -\int_0^p \nabla_p \cdot \mathbf{v}\, dp \tag{3.39}$$

is obtained.

And for local tendency at the level at which pressure p prevails

$$\frac{\partial p}{\partial t} = -\int_0^p \nabla_p \cdot \mathbf{v}\, dp - \mathbf{v}^* \cdot \nabla p + g \varrho w. \tag{3.40}$$

The right-hand second term which reflects the direct change effect in the case of ageostrophic motions across the isobars is normally small with an average order of magnitude of 1 hPa per day (see (3.31)). Since w vanishes in the case of flat terrain, the following therefore applies approximately for surface pressure tendency

$$\frac{\partial p_0}{\partial t} \approx -\int_0^{p_0} \nabla_p \cdot \mathbf{v}\, dp. \tag{3.41}$$

The pressure tendency on the surface is therefore chiefly determined by the vertical integral over isobaric wind divergence. The surface pressure falls if divergence prevails on the pressure surfaces and rises if convergence prevails.

From the above relation the following is true for geopotential tendency on pressure surfaces

$$\frac{\partial \Phi}{\partial t} = -\frac{1}{\varrho}\int_0^p \nabla_p \cdot \mathbf{v}\, dp - \mathbf{v}^* \cdot \nabla_p \Phi + g w. \tag{3.42}$$

The geopotential falls accordingly with

a) Horizontal divergence in the integral above the pressure interval between p and p=0,
b) Ageostrophic motion from the low to high geopotential and/or
c) Descending motion through the pressure surface.

The second term disappears in the case of motion parallel to the contours.

3.4 The vorticity equation

By crosswise differentiation of the equation of motion, the vorticity equation is obtained which gives information on the time-related change of the rotatory component of the horizontal wind.

$$\frac{d\eta}{dt} = -\eta \nabla_p \cdot \mathbf{v} + \mathbf{k} \cdot \left(\frac{\partial \mathbf{v}}{\partial p} \times \nabla_p \omega\right) \tag{3.43}$$

applies in the case of a frictionless motion in the p-system.

The first right-hand term is called the divergence term. It can be split up into

$$-\eta \nabla_p \cdot \mathbf{v} = -\zeta \underset{A}{\nabla_p \cdot \mathbf{v}} - f \underset{B}{\nabla_p \cdot \mathbf{v}}. \tag{3.44}$$

Part A is effective if the particles already have relative rotation. In this case isobaric convergence leads to increase, isobaric divergence to decrease of vorticity irrespective of the sign. This is identical with the conservation of momentum of rotation, here applied to the rotation around a vertical axis relative to the earth.

Part B describes the creation of vorticity by the Coriolis force. As can be read from Fig 3.16 pull to the right through this force in the case of convergence leads to cyclonic, in the case of divergence to anticyclonic rotation. This process is the most important form of creation of vorticity in systems of the large scale.

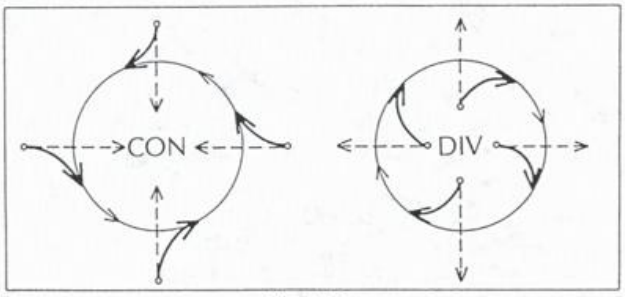

Fig. 3.16
Creation of relative vorticity by horizontal convergence or divergence

If the particles possess positive relative vorticity, Parts A and B have the same sign and reinforce each other. In the case of negative relative vorticity, however, compensation takes place. If in this case ζ remains quantatively less than f, B is dominant, if it exceeds f, A is dominant. If the amounts are the same, A and B cancel each other. This is also clear in the sum

$$-\eta \nabla_p \cdot \mathbf{v},$$

in which the sign and amount of absolute vorticity together decisively determine the time-related change. In the case of positive η, convergence leads to time-related vorticity increase, divergence to time-related vorticity decrease of the particles whereby the rate of change increases with η. In the case of $\eta < 0$ the opposite changes result while in the case of $\eta = 0$, i.e. $\zeta = -f$, divergence is unable to have any effect on vorticity change.

Assuming dynamic stability (see 2.11) it can be assumed that the particles will generally possess positive absolute vorticity. If the time-related change is only looked at with the divergence term

$$\frac{d\eta}{dt} = -\eta \nabla_p \cdot \mathbf{v},$$

$$\frac{d \ln \eta}{dt} = -\nabla_p \cdot \mathbf{v},$$

can also be written, which, in the case of time-related constant divergence, produces when integrated

$$\eta = \eta_0 \, e^{(-\overline{\nabla_p \cdot \mathbf{v}})t} \tag{3.45}$$

Vorticity then changes exponentially where, however, the various effects of terms A and B are manifest. With the typical magnitude of divergence during synoptic developments of $10^{-5} s^{-1}$, $10^5 s \sim 1$ day for the time results in which the original vorticity has increased through convergence times the e factor or reduced through divergence to the e-th part.

The second right-hand term in (3.43) is called the twisting term. It describes the conversion of rotation around a horizontal axis into rotation around the vertical axis by horizontal gradients of the vertical velocity. Its effect is explained in Fig 3.17 which diagramatically shows a cross-section through a zonal current increasing with height. With $\partial u / \partial p < 0$ this flow contains strong vertical shear and therefore rotation around the y-axis. If horizontally varying vertical motions now begin (with $\partial \omega / \partial y < 0$), the position of the isotachs originally lying isobarically changes and shear vorticity arises which is cyclonic in the case assumed here.

As a special example of the vorticity equation, the condition of a horizontal divergence-free current should be mentioned. In this case both forcing terms on the right side of (3.43) disappear and the particles keep their absolute vorticity. Along their trajectory changes from relative to planetary vorticity and vice-versa are possible (see 10.2).

Otherwise in the case of a time-related vorticity change naturally alternation between shear and curvature vorticity is possible. It can be shown (PICHLER [8]) that the change is determined by the term

$$\pm \left[K_t V \frac{\partial V}{\partial s} + \frac{\partial}{\partial n} \left(\frac{\partial \Phi}{\partial s} \right) \right]$$

or (3.46)

$$\pm \left[K_t V \frac{\partial V}{\partial s} - \frac{\partial}{\partial n} \left(\frac{dV}{dt} \right) \right].$$

With a positive sign transition from curvature to shear is described, with negative sign transition from shear to curvature is described. Important here on the one hand is velo-

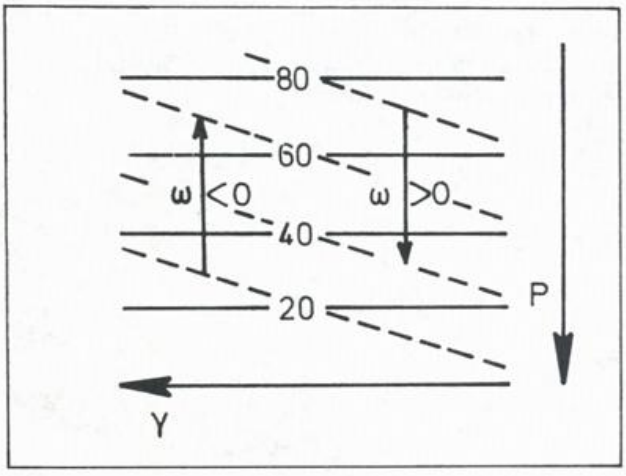

Fig. 3.17
Effect of the twisting term

city divergence. If it is positive, which is normally observed in a confluence zone, curvature vorticity changes to shear vorticity; if it is negative (diffluence zone), conversely transition from shear to curvature vorticity occurs. The other factor is ageostrophic motion across the isohypses which lead to changes in speed of the particles. If these changes vary across the current, transition from shear to curvature or vice-versa occurs depending on the particular distribution.

Resolved in accordance with the local time-related tendency of relative vorticity, the equation of vorticity reads

$$\frac{\partial \zeta}{\partial t} = -\mathbf{v}\cdot\nabla_p \eta - \omega\frac{\partial \zeta}{\partial p} - \eta\,\nabla_p\cdot\mathbf{v} + \mathbf{k}\cdot\left(\frac{\partial \mathbf{v}}{\partial p}\times\nabla_p\,\omega\right). \tag{3.47}$$

In addition to divergence term and twisting term, horizontal advection of absolute vorticity and vertical advection of relative vorticity also appear here. Advection of absolute vorticity which will be called A_η can be split up further into advection of relative and advection of planetary vorticity (A_ζ, A_f):

$$\begin{aligned} -\mathbf{v}\cdot\nabla_p\,\eta &= -\mathbf{v}\cdot\nabla_p\,\zeta - \mathbf{v}\cdot\nabla_p\,f \\ &= -\mathbf{v}\cdot\nabla_p\,\zeta - v\,\beta \end{aligned} \tag{3.48}$$

with $\beta \equiv \dfrac{\partial f}{\partial y}$, the ROSSBY parameter introduced in 3.13.

A positive vorticity tendency results through these three advection terms if either

a) The horizontal wind brings in particles with greater relative vorticity ,
b) The horizontal wind has a meridional component to the south ($v<0$) or
c) Particles with greater relative vorticity reach the pressure level concerned by vertical motions.

A negative tendency results in the case of negative horizontal or vertical advection and also if the wind has a meridional component to the north ($v>0$).

Finally the individual terms of the equation of vorticity for the large scale will be estimated whereby $L=10^6$m, $\Delta p=10^3$hPa, $\Delta\omega=10^{-3}$hPas^{-1}, $f=10^{-4}$s^{-1} and $\beta=10^{-11}$m^{-1}s^{-1} are used.

For the horizontal speed U, on the one hand the value typical for the lower troposphere 10 ms^{-1}, on the other hand the value characteristic of the jet stream 50 ms^{-1} is used. Therefore the following result

$$\begin{aligned} \frac{\partial \zeta}{\partial t},\ u\frac{\partial \zeta}{\partial x},\ v\frac{\partial \zeta}{\partial y} \sim \frac{U^2}{L^2} &= 10^{-10}/10^{-9}\ s^{-2} \\ v\,\beta \sim U\,\beta &= 10^{-10}\ s^{-2} \\ f\,\nabla\cdot\mathbf{v} \sim f\frac{U}{L} &= 10^{-9}\ s^{-2} \\ \zeta\,\nabla\cdot\mathbf{v} \sim \frac{U^2}{L^2} &= 10^{-10}/10^{-9}\ s^{-2} \\ \frac{\partial \omega}{\partial y}\frac{\partial u}{\partial p} - \frac{\partial \omega}{\partial x}\frac{\partial v}{\partial p} \sim \frac{\Delta\omega}{\Delta p}\frac{U}{L} &= 10^{-11}\ s^{-2} \\ \omega\frac{\partial \zeta}{\partial p} \sim \frac{\Delta\omega}{\Delta p}\frac{U}{L} &= 10^{-11}\ s^{-2}. \end{aligned} \tag{3.49}$$

It is seen that twisting term and vertical advection are one power of ten smaller than all other terms. They are, therefore, mainly neglected for practical use of the equation of vorticity in the large scale. Nevertheless, in individual cases or with processes in a relatively small area, they can be very significant. Using magnitude of 10^{-6}s^{-1} for the divergence, the term $\zeta\,\nabla\cdot\mathbf{v}$ also becomes very small and can be neglected compared with $f\,\nabla\cdot\mathbf{v}$ (see. 12.2)

3.5 Potential vorticity

In the case of adiabatically working processes, the air particles move on isentropic surfaces which they cannot leave. As, therefore, no motion component normal for isentropic surfaces exists, the vorticity equation in the Θ-system has the simple form

$$\frac{d\,\eta_\Theta}{dt} = \frac{\partial\,\zeta_\Theta}{\partial t} + \mathbf{v}\cdot\nabla_\Theta\,\eta_\Theta = -\eta_\Theta\,\nabla_\Theta\cdot\mathbf{v}. \tag{3.50}$$

Alternatively this can be written as

$$\frac{d\,\eta_\Theta}{dt} = -\frac{\eta_\Theta}{A}\frac{d\,A}{d\,t}$$

whereby A here represents the cross section of an isentropically flowing particle. From this results further

$$\frac{d}{dt}(A\,\eta_\Theta) = 0 \quad\text{or}\quad A\,\eta_\Theta = \text{const.}, \tag{3.51}$$

following the motion of the particle. The product of absolute vorticity and cross section magnitude is therefore constant in the case of adiabatic motion. If the cross section of the particles increases by isentropic divergence, their absolute vorticity becomes less; if A decreases by isentropic convergence, η_Θ must increase and vice versa.

If an air particle is examined between the isentropic surfaces Θ and $\Theta+\delta\Theta$, its mass is given by:

$$M = \varrho\,A\,\delta z$$

and, as

$$\delta z = \frac{\delta p}{g\,\varrho}, \qquad M = \frac{A\,\delta p}{g}.$$

The mass remains constant during motion so that

$$A = \frac{g}{\delta p}\,\text{const.} \quad\text{or}\quad A = \frac{g\,\delta\Theta}{\delta p}\,\text{const.},$$

is obtained, as $\delta\Theta$ also represents a constant. Under consideration of (3.51) this leads to

$$g\left(\frac{\eta_\Theta}{\delta p}\right) = \text{const.} \quad\text{or}\quad g\,\eta_\Theta\left(-\frac{\partial\Theta}{\partial p}\right) = \text{const.}, \tag{3.52}$$

following the motion.

The quotient $g\left(\dfrac{\eta_\Theta}{\delta p}\right)$ is described as isentropic potential vorticity (IPV). It remains conservative within an adiabatic air flow. This means an increase in vorticity produces an enlargement of the layer thickness between the isentropic surfaces and conversely a decrease of vorticity is associated with a reduction of this layer thickness. This is equally important with a change in thermal stratification as the alternative form of the equation shows. With an increase of vorticity, thermal stability is weakened accord-

ingly by vertical stretching, with decreasing vorticity, however, it is increased by vertical shrinking. Conversely it is true that in an area where the current flows out into a stable zone of crowded isentropic surfaces, the air particles gain anticyclonic vorticity (through isentropic divergence) while they develop marked cyclonic rotation through convergence when entering an area with greater layer thickness.

3.6 Circulation and circulation theorem

In many considerations not only is rotation of the particles around a vertical axis interesting, but also around horizontal or any direction oriented axes. They are mathematically recorded by the rotor

$$\nabla_3 \times \mathbf{v}_3$$

of the velocity field whose vertical component represents relative vorticity.

As an alternative to this a macroscopic measure for rotational motion components can be defined. Here a closed curve in space is considered. As a result of tangential wind components, this curve can be changed into rotational motion. A statement is obtained in this connection by the curve integral formed over this wind component (see Fig 3.18).

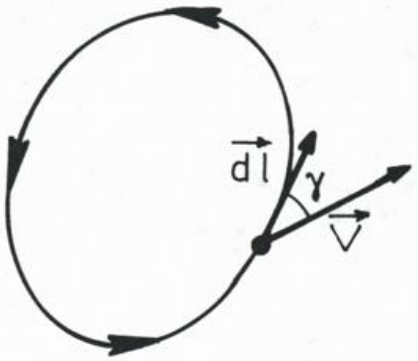

Fig. 3.18
(See text)

$$C = \oint \mathbf{v}_3 \cdot \mathrm{d}\mathbf{l} = \oint \mathbf{V}_3 \cos\gamma \, \mathrm{d}l \tag{3.53}$$

C is the circulation. It is positive if rotational motion runs in the direction of integration, i.e. anti-clockwise, negative if it runs clockwise.

In the case of horizontally oriented curves, the same sign results as in the case of relative vorticity i.e. circulation is positive for cyclonic, negative for anticyclonic rotation.

Information about the time-related change of circulation is obtained by applying the curve integral to the three-dimensional equation of motion for a frictionless current

$$\oint \frac{\mathrm{d}\mathbf{v}_3}{\mathrm{d}t} \cdot \mathrm{d}\mathbf{l} = -\oint \alpha \nabla_3 p \cdot \mathrm{d}\mathbf{l} - \oint (2\boldsymbol{\Omega} \times \mathbf{v}_3) \cdot \mathrm{d}\mathbf{l} + \oint \mathbf{g} \cdot \mathrm{d}\mathbf{l}. \tag{3.54}$$

For the lefthand integrands

$$\frac{\mathrm{d}\mathbf{v}_3}{\mathrm{d}t} \cdot \mathrm{d}\mathbf{l} = \frac{\mathrm{d}}{\mathrm{d}t}(\mathbf{v}_3 \cdot \mathrm{d}\mathbf{l}) - \mathbf{v}_3 \frac{\mathrm{d}}{\mathrm{d}t}(\mathrm{d}\mathbf{l})$$

can be written and, as $\mathrm{d}\mathbf{l}/\mathrm{d}t = \mathbf{v}_3$,

$$\frac{\mathrm{d}\mathbf{v}_3}{\mathrm{d}t} \cdot \mathrm{d}\mathbf{l} = \frac{\mathrm{d}}{\mathrm{d}t}(\mathbf{v}_3 \cdot \mathrm{d}\mathbf{l}) - \mathbf{v}_3 \cdot \mathrm{d}\mathbf{v}_3.$$

The curve integral of a total differential disappears so that

$$\oint \mathbf{v}_3 \cdot \mathrm{d}\mathbf{v}_3 = \frac{1}{2} \oint \mathrm{d}(\mathbf{v}_3 \cdot \mathbf{v}_3) = 0.$$

As also the last term in (3.54) is zero, it follows

$$\frac{\mathrm{d}C}{\mathrm{d}t} = \frac{\mathrm{d}}{\mathrm{d}t} \oint \mathbf{v}_3 \cdot \mathrm{d}\mathbf{l} = -\oint \alpha \nabla_3 p \cdot \mathrm{d}\mathbf{l} - \oint (2\boldsymbol{\Omega} \times \mathbf{v}_3) \cdot \mathrm{d}\mathbf{l}. \tag{3.55}$$

The term $(2\boldsymbol{\Omega} \times \mathbf{v}_3) \cdot \mathrm{d}\mathbf{l}$ can be changed to $(\mathbf{v}_3 \times \mathrm{d}\mathbf{l}) \cdot 2\boldsymbol{\Omega}$. The amount of vector $\mathbf{v}_3 \times \mathrm{d}\mathbf{l}$ is $V_N \, \mathrm{d}l$ whereby V_N represents the wind component normal to the curve. Therefore $\oint V_N \, \mathrm{d}l$ represents expansion of the area which is enclosed by the curve, per unit time. With A as magnitude of the area and n as unit vector along the normals directed outwards, the following results:

$$-\oint (2\boldsymbol{\Omega} \times \mathbf{v}_3) \cdot \mathrm{d}\mathbf{l} = -\frac{\mathrm{d}}{\mathrm{d}t}(A\,\mathbf{n} \cdot 2\boldsymbol{\Omega}).$$

If the angle between the rotation axis ($\boldsymbol{\Omega}$) and the normals ($\mathbf{n}$) directed outwards is described with ψ, we obtain (see Fig 3.19)

$$A\,\mathbf{n} \cdot 2\boldsymbol{\Omega} = 2\Omega A \cos\psi.$$

On the other hand $A\cos\psi$ is the projection of A onto the equatorial plane which will be described as A_E. Therefore the circulation theorem of V. BJERKNES is obtained in the form

$$\frac{\mathrm{d}C}{\mathrm{d}t} = -\oint \alpha \, \mathrm{d}p - 2\Omega \frac{\mathrm{d}A_E}{\mathrm{d}t}. \tag{3.56}$$

It describes the time-related change in circulation relative to the rotating earth.

The first right-hand term is called the solenoid term. Solenoids are square tubes which result if the surfaces of equal pressure (isobaric surfaces) and equal specific volume (isosteric surfaces) intersect in space. It can be easily seen that the expression $-\oint \alpha \, \mathrm{d}p$ is equal to the number N of the isobaric-isosteric solenoids embraced by the curve.

For this purpose the curve ABCD in Fig 3.20 which runs along two isobaric and two isosteric surfaces is examined. The following contributions to the curve integral along the individual parts result:

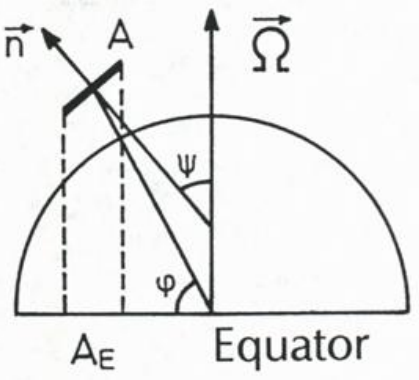

Fig. 3.19
(See text)

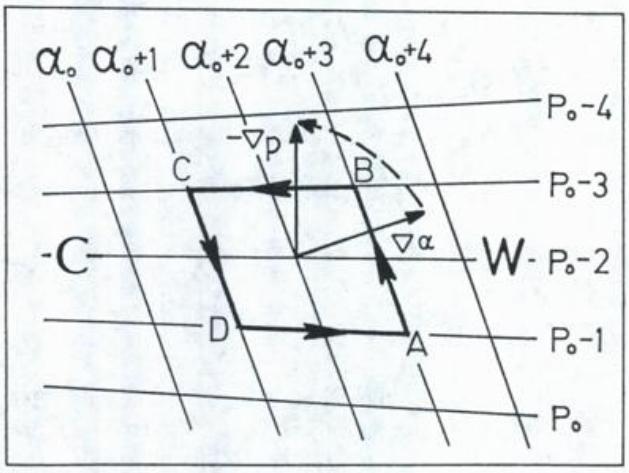

Fig 3.20
(p, α)-Solenoids embraced by the curve ABCD

A→B: $p_0 - 1 \rightarrow p_0 - 3$ with $\alpha_0 + 3$
contribution $2(\alpha_0 + 3)$
B→C: $p_0 - 3$ const.; $dp = 0$
C→D: $p_0 - 3 \rightarrow p_0 - 1$ with $\alpha_0 + 1$
contribution $-2(\alpha_0 + 1)$
D→A: $p_0 - 1$ const.; $dp = 0$

Therefore as total sum results:

$$2\alpha_0 + 6 - 2\alpha_0 - 2 = 4,$$

which corresponds exactly to the number of solenoids embraced by the curve.

As N is always positive when solenoids are present, the solenoid term causes positive circulation acceleration which is directed from the ascendent of the specific volume $\nabla_3 \alpha$ to the gradient of pressure $-\nabla_3 p$. As a result, the warmer air is accelerated to the lower and the colder air to the higher pressure. If circulation is vertically oriented, the warmer air in it is lifted and set in motion aloft towards the colder air, while the colder air at the same time subsides and at a lower level pushes forward towards the area of the warmer air. Such circulation is described as solenoidally direct. As the denser mass in it descends and the less dense mass rises, the centre of gravity of the whole system moves downwards. This is synonymous with a reduction of potential energy and its conversion into kinetic energy of the circulation motion. This energy transformation forms the main source of all atmospheric motions – from small area circulation of the sea breeze, e.g., right up to the large scale eddies of cyclones and anticyclones. However, this kind of energy conversion is only possible in the case of baroclinic stratification as in the case of barotropy isobaric and isosteric surfaces lie parallel in space and therefore no solenoids exist.

Using the equation of state (1.1) the solenoid term can be converted.

$$N = -\oint \alpha \, dp = -\oint R_d \, T \, d \ln p, \qquad (3.57)$$

applies so that isothermic and isobaric surfaces can also be used to calculate solenoid acceleration. In addition

$$N = \oint c_p \, T \, d \ln \Theta \qquad (3.58)$$

is obtained using the definition equation of potential temperature (1.5).

The solenoid number results accordingly from the spatial distribution of isothermic and isentropic surfaces (see Fig 3.21).

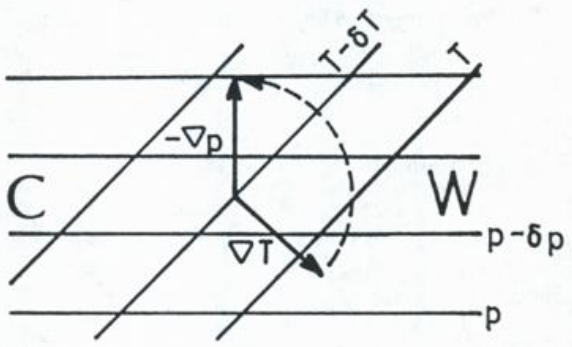

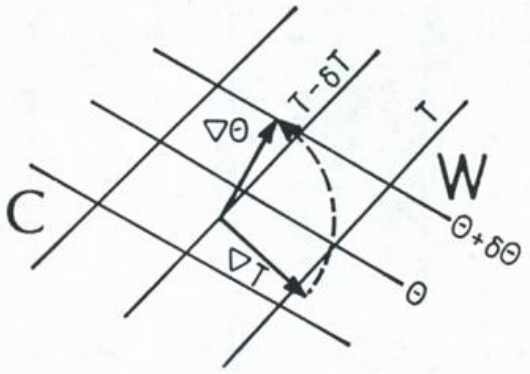

Fig 3.21
Solenoid representation by means of p and T or T and Θ

The term

$$-2\Omega \frac{dA_E}{dt}$$

is described as the Coriolis effect as it contains the influence of the earth's rotation. It produces a contribution to circulation acceleration relative to the earth under the following conditions:

a) In the case of horizontally oriented surfaces, the area content reduces through horizontal convergence. With $dA_E/dt<0$ it becomes $dC/dt>0$ and positive (cyclonic) circulation results. Conversely in the case of horizontal divergence with $dA_E/dt>0$ and $dC/dt<0$, negative (anticyclonic) circulation is set in motion.
b) In the case of motion of a horizontally oriented surface with constant content to the equator, A_E reduces and cyclonic circulation results. In the case of motion to the pole on the other hand A_E increases and anticyclonic circulation is triggered.
c) As a result of horizontally differing vertical motions, the spatial orientation of a curve and the surface enclosed by it are changed. As a result the magnitude of

A_E also changes due to which corresponding circulation accelerations take place.

These statements correspond qualitatively to the statements of the vorticity equation (3.43).

As already detailed, the energy for most atmospheric motions comes from acceleration by the solenoid term. However, once these motions have started, acceleration is mostly reduced, as the Coriolis effect works in a compensating way. As an example of this, a baroclinic flow is considered, which should be in geostrophic equilibrium. Due to the solenoids, positive circulation acceleration occurs for each vertical and across the flow oriented surface. On account of the vertical wind differences, however, the curve at the same time inverts and the surface expands so that the Coriolis effect produces a negative acceleration contribution which competes with the positive contribution of the solenoids. Only if the equilibrium is disturbed by any kind of process, circulation across the flow can start by outweighing one of the two terms.

4 Air masses

Observations show that the meridional temperature contrast between pole and equator is not uniformly distributed. There are rather large areas which are filled by relatively uniformly heated air, divided by zones where wide temperature differences occur within a short distance. Apart from temperatures, such discontinuous distribution also applies in the case of other characteristics of the air particles. The large scale air volumes of uniform character are described as air masses, while the terms front and frontal zone have been introduced for the transition zones.

4.1 Origin, classification and characteristics of air masses

The ability to define and classify air masses in a clear way can be traced back to the fact that within the general circulation, larger quantities of air are subject for longer periods to the same conditions in regard to radiation and exchange with the earth surface and at the same time mostly acquire similar characteristics such as temperature and humidity content, vertical temperature gradients, content of pollution etc. Determining factors for this process are the geographic latitude, type of ground – and here especially the land-sea distribution – as well as the prevailing system of horizontal motion in the area concerned. In addition the effect of the predominant vertical motion is of importance in free atmosphere. Large quasi-stationary anticyclones are seen especially as „source areas" for the air masses.

In lower latitudes on account of heat excess, warm air masses are produced, in high latitudes on account of heat deficit, cold air masses are produced. In regard to the type of the underlying surface, oceans play a special role. On account of high heat storage, but above all on account of the large heat conductivity of moved water caused by turbulent exchange, the surface temperature of large sea surfaces only has minimum seasonal variation. The oceans therefore work generally in the winter as heat source but in the summer as heat sink for the air passing over them. In addition the oceans naturally form the main reservoir for evaporation and water vapour transport into the atmosphere.

To typify and distinguish the individual air masses, variables such as pseudo-potential or equivalent potential temperature are generally used. They also include the humidity content of air with the available condensation heat and are invariant with vertical motion including condensation or evaporation.

Corresponding to the concept of the „polar front theory" (see Section 8.1), only two main air masses were distinguished earlier – the cold and dry polar air coming from the heat deficit region of the high latitudes and the warm and moist tropical air produced in the southern regions of excess heat – on both sides of a front, even the polar front. According to the state of equilibrium a strongly baroclinic front of this type must be associated with a high tropospheric strong wind field which has later been proven by aerological soundings and described as „polar front jet stream". The ascents also showed, however, that south of the polar front a further baroclinic zone exists, connected with a second extraordinarily powerful and persistent strong wind field, the sub-tropical jet. In addition it has been shown that the circulation of lower latitudes (Hadley circulation) for the most part runs enclosed within itself, so that air masses, which actually originate in the tropics, only sometimes reach the west wind zone.

Using the diagram of general circulation (see Fig 4.1, according to PALMEN and NEWTON [9]), three main air masses are therefore distinguished today: polar air (PA), tropical air (TA), and a middle air mass strongly varying in character, which is described as temperate air and is typical for the west wind zone of the more central latitudes (MLA mid-latitude air). These three air masses are only weakly baroclinic or even barotropic and are separated by the strongly baroclinic zones of the polar front – between polar air and temperate air – and the sub-tropical front – between temperate air and tropical air. In the middle troposphere (500 hPa) the mean position of the polar front varies according to season between 40° and 70°N, that of the subtropical front between 30° and 45°N.

The contrast between TA and MLA is, however, mainly concentrated front-like only in the upper troposphere, where northerly penetrating tropical air within the Hadley circulation converges with MLA air. In the lower troposphere, however, no clear air mass division between both air masses generally develops on account of the prevailing

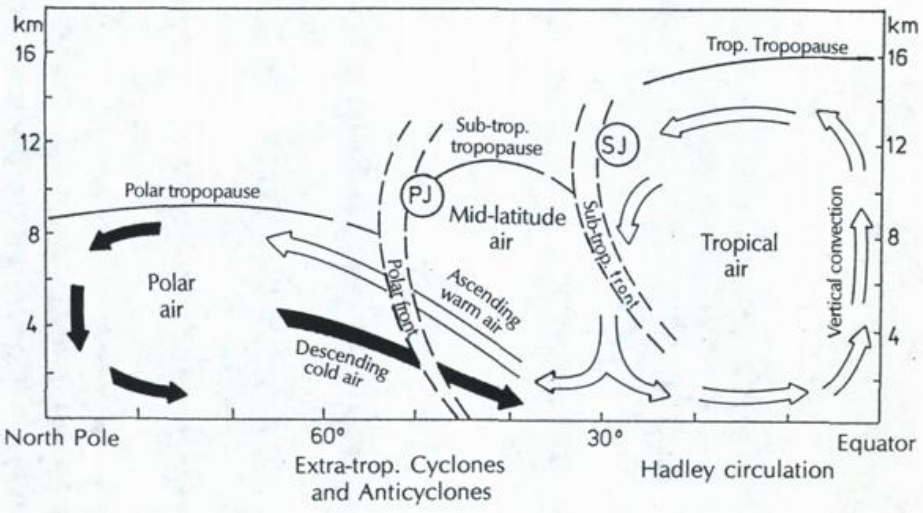

Fig. 4.1
Distribution of air masses, fronts and jet streams in the northern hemisphere in winter. According to PALMÉN and NEWTON [9]

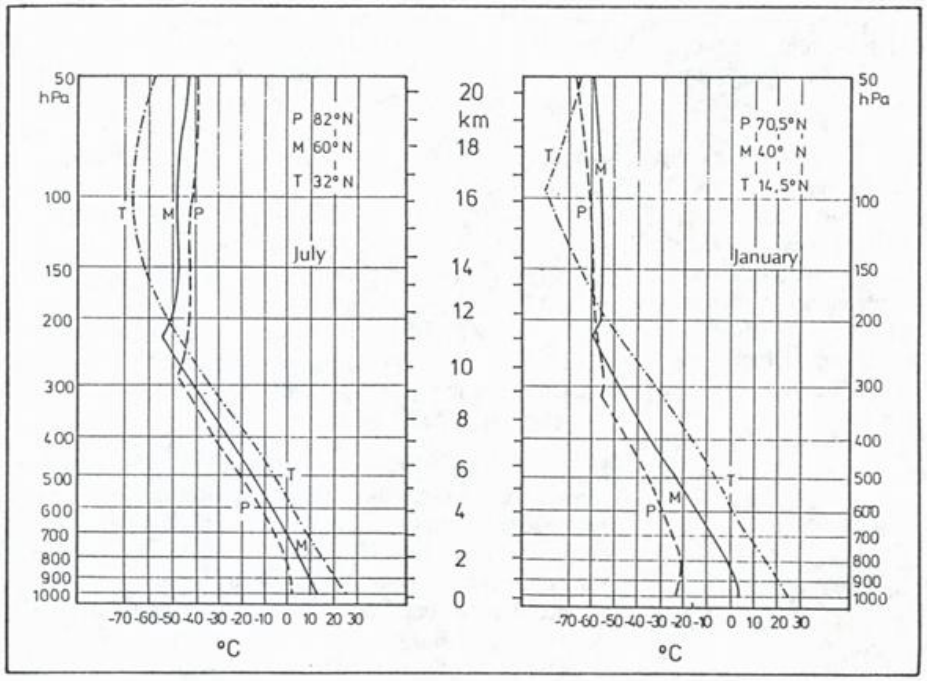

Fig 4.2
Characteristic vertical temperature distribution in the three main air masses in summer and winter. According to DEFANT [10]

horizontal divergence of the stream field (see Section 7: frontogenesis).

In contrast to this, the baroclinic zone of the polar front normally reaches as far as the surface or is especially strongly marked in the lower troposphere, and the contrast between PA and MLA frequently shows itself with extraordinary sharpness in the form of line-like surface fronts. This applies especially to the area of the cyclones where frontal contrasts are maintained by horizontal convergence, while weakening and dissipation of the surface fronts occur regularly in the area of high pressure regions as a result of divergence.

In regard to temperature-related characterization of the three main air masses, typical vertical distributions are reproduced in Fig 4.2 which have been obtained by DEFANT [10]. It is seen that, within the troposphere, the temperature difference between the three masses is 5–10 K in summer, while in winter it increases and exceeds 20 K near the ground. The greatly differing height situation of the tropopause is characteristic. In the area of the two frontal zones, consequently, a break zone of the tropopause, with sudden change in height, occurs (see also Fig 5.8).

It can be further seen from the temperature curves that the polar air is the most stable of the three main air masses. In the middle troposphere the vertical temperature gradient in it is 0.6 K/100 m. Especially striking, however, is the isothermic or inverse stratification below 2 km height, which greatly restricts vertical exchange. It can be traced back to the fact that diabatic cooling, to which this air mass is subject, is at its greatest near the ground, especially of course in winter and over snow-covered land or the frozen surfaces of the Arctic. In summer the melting processes prevent large temperature increases above 0°C. On account of its low temperature, the polar air can only absorb little water vapour. But also the inclusion of additions which, for example, can act as condensation cores is normally negligible. As a consequence, the horizontal visibility is mostly very good. The tropopause has an average height of 9 km and temperatures around -50°C in the polar air. In the stratosphere this air mass is at its warmest in summer, while in winter it is colder than the temperate air on account of lack of radiation at high latitudes.

The tropical air, being the tropospherically warmest air mass, is at the same time the one with the least static stability. The vertical temperature decrease is 0.7–0.8 K/100 m in the middle between the ground and a height of 13 km. At this height the secondary, at about 16 km height, the actual tropical tropopause is located with temperatures near -70°C in summer and around -80°C in winter. In the stratosphere this mass is therefore the coldest of the three main air masses. On account of evaporation from the ocean surfaces, the tropical air in the lower troposphere generally has a high moisture content. As a result of this, the vertical profile of the pseudo-potential temperature is also determined, which has maximum values nearest the ground and a minimum at 700–500 hPa. The stratification is consequently potentially unstable (see 2.2). Instability is triggered when the tropical air reaches the rising branch of the Hadley circulation above the Intertropical Convergence Zone (ITCZ). There deep cumulonimbi form in this case which mostly arrange themselves into large area cloud masses, so-called „cloud clusters". Further northwards, however, very dry air can be found in the middle troposphere on account of the predominant subsiding motion. It is separated from the moisture-laden air near the ground by the „Passat inversion" which is located at a height of 1–2 km above the ground. Only flat cumulus clouds can form under it.

The temperate air of the middle latitudes is the air mass with the least uniform characteristics. The reason for this lies in the fact that this mass is always enclosed in the west wind zone with more or less fast motion, whereby it is subject to strong changes as a result of influences from the ground, but especially also as a result of vertical motion of the moving cyclones and anticyclones in this area. These processes are described in more detail in the following sec-

tion. It can be seen from the temperature curves in Fig 4.2 that the vertical temperature gradient in the temperate air is around 0.7 K/100 m and the tropopause has a temperature of around -55°C at a height of 11 km.

In regard to the weather conditions in the west wind zone the air mass difference between polar air and temperate air is of major importance in accordance with what has just been stated above. However, tropical air from the Hadley circulation repeatedly penetrates into the westwind zone. Near the surface these intrusions occur mainly on the west fringe of the high pressure areas of the sub-tropical high pressure belt – i.e. for example on the west fringe of the Azores high. With height tropical air can be transported far to the north if waves of greater amplitude have formed inside the upper current. On account of the vertical change of wind direction connected with temperature advection, relative motions from differing directions occur in this case at various levels, so that tropical air with height can pass over temperate or polar air in the lower layers, or vice versa. From this air mass stratification, thermal stability is naturally clearly determined and resulting from this also the character of the weather in the area concerned.

Within the polar air another second, but limited to the lower troposphere, frontal zone can be made out in winter, which is called the arctic front. It separates the extreme cold air of the areas near the pole from the less cold air masses in the south and frequently is fixed orographically on coastlines and the pack ice boundary. In addition its position is greatly influenced by the extent of snow cover on continental land. As the baroclinic zone of the arctic front remains restricted to the lower troposphere, it does not appear useful to define „arctic air" in addition to polar air. Also, it would be very difficult in individual cases to distinguish between air which actually comes from arctic regions and equally cold or colder air which originates far to the south in the area of an anticyclone over snow-covered continental land.

4.2 Air mass transformation

The same processes such as radiation, turbulent exchange and vertical motion, which lead to the origin of typical characteristics of the air masses at their source, cause faster or slower or greater or smaller changes in the way they appear when the air masses move from the source area and are transported within the moving pressure systems and waves. The processes taking place here are described as air mass transformation.

A noticeable change in an air mass can already occur if the force of the vertical exchange due to turbulence in it, changes significantly. This occurs, for example, if a polar air mass comes into the circulation system of a depression from the weak wind area of a winter anticyclone and as a result is more thoroughly mixed. As turbulence tries to create uniform distribution of the air mass characteristics with constant levels of potential temperature and mixing ratio, mixing leads to a rise in temperature and reduction in relative humidity near the ground, as well as to cooling and increased humidity in the upper part of the layer affected by mixing. As a result the inversion on the ground is dissipated, while a new one forms above the mixed layer. The increased humidity aloft can give rise to the formation of St or Sc-cloud (see Fig 4.3a).

A very important transformation process is warming or cooling from the ground. In this respect again large sea areas play an important role. As the surface temperature of the ocean on account of good heat conductivity and heat storage mentioned earlier practically does not react to changes in air temperature, the oceans represent huge heat sources or heat sinks depending on the temperature of the air passing over them. However, the intensity of heat transfers from water to air or vice versa is dependent on the direction of the heat flux. During warming from the surface at the same time weakening of the thermal stability occurs as a result of which turbulent exchange is greatly increased while stabilisation which is associated with cooling leads to calming of the vertical turbulent motion. With otherwise similar conditions, therefore, heating of an air mass which passes over a warmer surface is considerably faster than cooling down of an air mass which passes over a cold surface. Turbulent warming soon covers a vertically thick area while cooling down remains limited to a shallow layer near the ground (Fig 4.3b).

In this process humidity plays an important role. Humidity is transported from the ocean surface into the normally dry air masses which originate from continental land. If the air mass is cooled down at the same time by the ground, relative humidity quickly increases inside the stable layer near the ground as a result of which visibility becomes worse and fog can arise. With simultaneous warming and destabilization of the air mass, the increase in humidity causes convective clouds to form. As a result of the condensation heat released in these clouds, higher air layers are also included in the transformation process and warmed up (Fig 4.3c).

Radiation works as a transformation factor mainly if the air masses are situated over continental land. In the case of fair

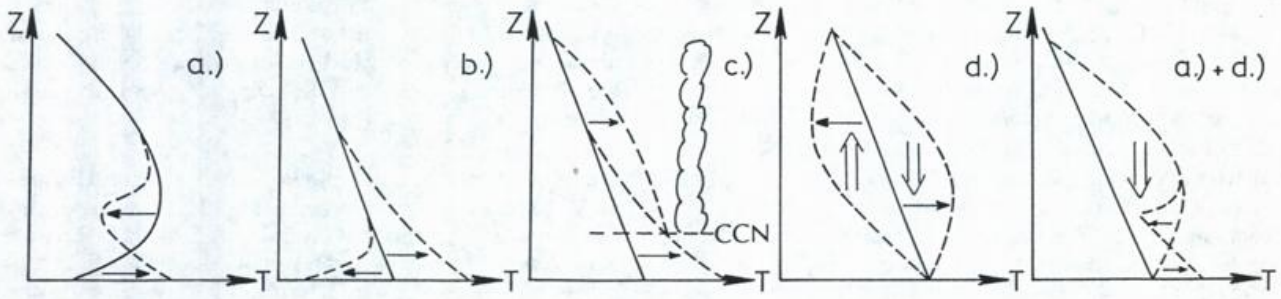

Fig 4.3
Air mass transformation by a) turbulent mixing b) diabatic heat transfers from and to the ground c) release of latent heat d) stretching and shrinking

weather in summer, air is heated by the ground progressively from day to day – associated with destabilization and reduction of relative humidity, in winter conversely the air layers near the ground cool down progressively with stabilisation and increase in humidity.

A clear example of the influence of radiation on air mass transformation has been given by WEXLER [12]. He examined the temperature changes within marine polar air masses which flow with temperatures around freezing point and fairly moist adiabatic lapse rate from the North Pacific into the cold Yukon valley (Alaska) and there come under the influence of high pressure.

In the case of very weak winds, turbulent heat transfer is minimal so that radiation on the snow-covered ground surface can cause temperature reduction to -33°C in only two hours. Cooling remains in this case limited to an infinitesimal level which increases slowly through molecular heat conductivity.

At the upper level of the ground inversion which resulted thus, increased cooling then occurs so that an isothermic layer is formed which increases more and more with height. As counter-radiation now becomes less on the ground, further but slower cooling, which eventually leads to temperatures of -70°C, results there.

Fig 4.4 diagramatically shows several stages of the cooling process described and, for comparison, a temperature sounding from the area concerned.

PETTERSSEN [4] pointed out that dynamic processes are also of great importance for the change in air mass structure. The large scale vertical motions occurring in these processes influence the vertical temperature and humidity distribution to a large extent. Ascent leads to adiabatic cooling connected with an increase in relative humidity, eventual cloud formation and precipitation, descent leads to adiabatic warming with humidity reduction and cloud dispersion. The configuration is in this case generally such that the vertical motions are at their maximum in the middle troposphere while on the ground and at greater heights (jet stream or tropopause level) the motion is horizontal. As Fig 4.3d shows in the case of rising, vertical stretching linked with destabilization occurs in the lower troposphere and vertical shrinking linked with stabilisation in the upper troposphere. Destabilization can lead, in the case of sufficient humidity, to the fact that not only stratiform clouds but also deep cumulus clouds with showers and thunder are formed as a result of rising. Upper stabilisation can result in the tropopause newly forming at a lower level.

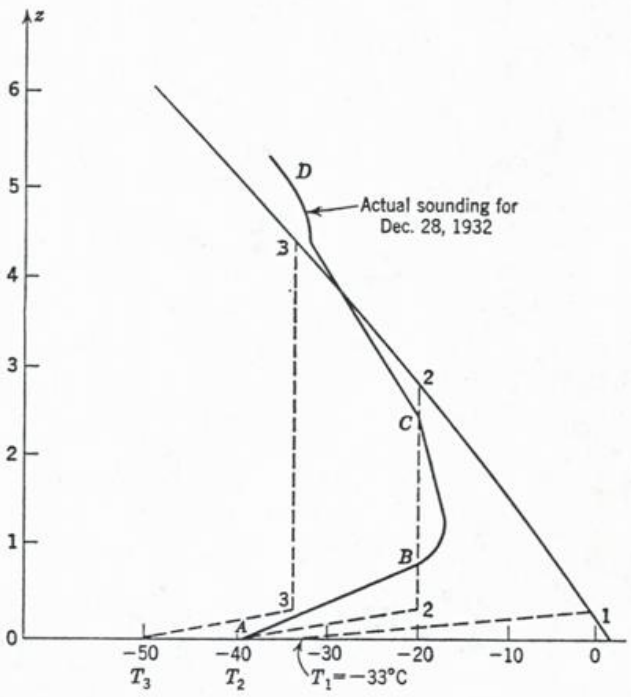

Fig 4.4
Various stages of transformation from marine to continental polar air. According to HALTINER and MARTIN [2]

In the subsidence area, on the other hand, destabilization aloft and stabilisation in the lower troposphere occur. As a result convective overturnings are prevented from leaving the ground or at least made more difficult. In conjunction with turbulent and convective vertical exchange, frequently stratification with a 1–2 km thick mixed layer arises and a powerful inversion with reduced humidity above this. In the upper part of the mixed layer, St or Sc fields or even single fine weather cumuli can form.

The influence of vertical motions will be demonstrated finally with the example of large-scale meridional air mass transport. The trajectories which are run through here by the particles are shown in idealised form in Fig 4.5. It is characteristic that the cold air and warm air streams flow apart in the meridional direction so that one part of the air masses moves along a heavily cyclonically curved trajectory, while another part moves along a heavily anticyclonically curved trajectory (see PALMEN and NEWTON [9]).

Assuming adiabatic motion, the conservation of potential vorticity (3.52) applies along these trajactories, i.e.

$$g\frac{(\zeta+f)}{\Delta p}=\text{const.},$$

following the motion. Δp here is the total vertical thickness of an air mass, i.e. for example polar air. In addition the shear vorticity will be neglected as against the curvature in further considerations.

If the polar air particles start in a straight line at 60°N, i.e. with $\zeta = 0$

$$r=\frac{\Delta p_{30}}{\Delta p_{60}}=\frac{\zeta_{30}+f_{30}}{f_{60}}$$

is obtained for ratio r of the vertical thickness at 60°N and 30°N.

The following ratios result from this for some selected values of ζ_{30}

ζ_{30}	$-\frac{1}{2}f_{30}$	0	$f_{60}-f_{30}$	f_{30}
r	0,3	0,6	1,0	1,2

It is recognised that considerable vertical shrinking of the cold air mass takes place along straight and anticyclonically curved trajectories, which must be linked with corresponding horizontal divergence. Along the cyclonically curved trajectory which has the relative vorticity $\zeta_{30} = f_{60} - f_{30}$ at 30°N, absolute vorticity remains constant. Along this trajectory the current remains divergence-free and the vertical thickness remains unchanged. In the area of air trajectories which have an even stronger cyclonic

curve at 30°N, however, the polar air expands vertically, linked with horizontal convergence.

With shrinking or stretching of the air masses, corresponding temperature and stability changes occur. Under the assumption that the polar air at 60°N reaches up to 300 hPa and has a temperature of -58°C there, the following pressure and temperature values along the straight trajectory can be calculated for the upper limit of the heavily shrinking air mass:

Latitude	60°	50°	40°	30°	20°	10°
Upper limit [hPa]	300	380	490	590	730	860
T [°C]	–58	–43	–26	–13	+4	+22

Adiabatic warming is so fast in the case of straight line trajectories that between 40° and 30°N at the latest the polar air has lost its original air mass character and, according to the temperature ratios in Fig 4.2, should be classified as MLA. If equally fast diabatic heat transfer does not take place near the ground at the same time, thermal stratification quickly stabilises (see Fig 4.3). If cumulonimbi could perhaps develop with showers and thunder originally in the deep polar air, at best the formation of flat fine weather cumuli is now possible. It is therefore seen that the whole appearance of an air mass can totally change with the dynamic processes resulting from air mass transport.

From this consideration, it also follows that polar air flowing southwards only maintains its vertical thickness in the case of cyclonic motion, whereby it again reverts sooner or later towards the pole. Deep polar air masses at low latitudes must therefore possess large cyclonic vorticity, which is confirmed in the form of isolated cold cyclones. Polar air, which follows anticyclonic trajectories, however, shrinks to a layer which becomes flatter and flatter. In the case of a sufficiently heavy curvature of the trajectories, this flat and adiabatically warmed cold air also turns again to the north and eventually comes under the influence of a cyclone, whereby its vertical thickness again increases.

In the case of a meridional cold air outbreak which follows the diagram in Fig 4.5, the thickness of the cold air on the east fringe, in the area of cyclonically curved trajectories must therefore be far greater than on the west fringe where the air trajectories run anticyclonically. On the east fringe of the cold air surge, the front surface will be accordingly more steeply oriented to the warm air than in its west part where the front changes into a quasi-horizontal inversion.

Conversely, warm air brought northwards (MLA or TA) only maintains its original thickness and thermal structure with anticyclonically trajectory curvature. Deep warm air at high latitudes must therefore have large anticyclonic vorticity – as, for example, in the form of isolated high pressure areas. Along straight or cyclonically curved trajectories on the other hand, a heavier or weaker vertical stretching of the warm air takes place, linked with horizontal convergence, adiabatic cooling aloft and destabilization of thermal stratification.

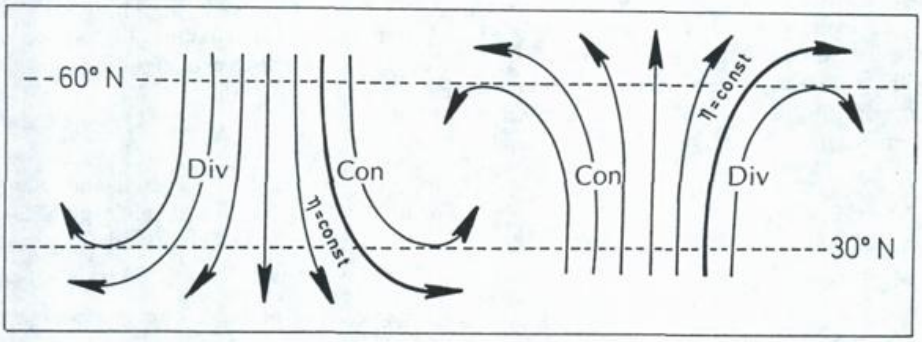

Fig 4.5
Idealized trajectories with meridional air mass transports. According to PETTERSSEN [4]